

The Structure, Preparation, Characterization, and Intercalation Mechanism of Layered Hydroxides Intercalated with Guest Anions

Zongkun Chen, Qiqi Fan, Minghua Huang,* and Helmut Cölfen*

Since the intercalation of anions into layered hydroxides (LHs) has a great impact not only on their nucleation and growth but also on their structure, composition, and size, the intercalation chemistry of LHs has aroused the strong interest of researchers. However, the progress in the fundamental understanding of LHs intercalated with guest anions have not been paralleled by a concomitant development of the preparation and performance improvement of such materials. Considering the guidance of a timely in-depth review for scientists in this area, a systematic introduction about the development that is made on the above-mentioned issues is highly needed but yet missing so far. Herein, recent advances in understanding the chemical composition and structure of LHs intercalated with guest anions are systematically summarized. Meanwhile, typical and emerging bottom-up synthesis methods of LHs intercalated with anions are reviewed, and the potential impact of external reaction parameters on the intercalation of anions into LHs are discussed. Besides, different analytical characterization techniques employed in the examination of guest anion-intercalated LHs are deliberated upon. Finally, although progress is slow in exploring the intercalation mechanism, as many examples as possible are included in this review and inferred the possible intercalation mechanism.

hydroxides with a layered structure, such as the alkaline earth hydroxides, transition metal hydroxides, and layered double hydroxides (LDH), have attracted intense interest in a wide range of applications,^[1c,2] such as catalysis,^[2b,3] energy storage,^[2d,4] light-emission,^[5] flame retardance,^[5b,6] etc. Various strategies are adopted to improve the performance of layered hydroxides (LHs) by tuning the microstructure,^[7] metal composition,^[8] crystallinity,^[9] and particle size.^[10] LHs possess the unique ability to accommodate various anions between interlayers.^[4a] Studying the intercalated anions represents a fast-growing and vital way to explore the fundamental understanding and to promote the practical application of LHs because the intercalation chemistry of LHs has great relevance with respect to nucleation, growth, composition, structure, and size. Considerable efforts have been made over the past decade to not only carry out the fundamental research related to LHs intercalated with guest anions but also summarize the recent advances in such field, and significant achievements have been obtained.^[4a,11] However, previous

studies have largely focused on the preparation of such materials and the impact of intercalated anions on performance for target applications. Progress in the fundamental understanding of LHs intercalated with anions, such as the structure, the maintenance of electrical neutrality, the analytical characterization techniques, and the intercalation mechanism, have not been paralleled by a concomitant development of the preparation and performance improvement for such materials. Such fundamental understanding is essential for both optimizing the synthesis conditions of LHs intercalated with guest anions and realizing the custom synthesis of LHs with the desired attributes. Therefore, undertaking efforts to address the above-mentioned issues is highly necessary. One in-depth review can serve as a reference guide for scientists in the area and help quickly capture the advances of LHs intercalated with guest anions in one place, and a systematic introduction of the progress that has been made about the fundamental understanding of LHs intercalated with guest anions is urgently needed but yet missing. To solve this problem, we systematically summarize the recent progress in the fundamental understanding of the LHs' intercalation chemistry. To be specific, the chemical composition

1. Introduction

Due to the easy preparation, flexible structural composition, tunable interlayer space, and unique physicochemical properties,^[1]

Z. Chen, Q. Fan, H. Cölfen
Physical Chemistry
University of Konstanz
Universitätsstraße 10, D-78457 Konstanz, Germany
E-mail: helmut.coelfen@uni-konstanz.de
M. Huang
School of Materials Science and Engineering
Ocean University of China
Qingdao 266100, China
E-mail: huangminghua@ouc.edu.cn

 The ORCID identification number(s) for the author(s) of this article can be found under <https://doi.org/10.1002/smll.202300509>

© 2023 The Authors. Small published by Wiley-VCH GmbH. This is an open access article under the terms of the Creative Commons Attribution License, which permits use, distribution and reproduction in any medium, provided the original work is properly cited.

DOI: 10.1002/smll.202300509

H																	He																												
Li	Be											B	C	N	O	F	Ne																												
Na	Mg											Al	Si	P	S	Cl	Ar																												
K	Ca	Sc	Ti	V	Cr	Mn	Fe	Co	Ni	Cu	Zn	Ga	Ge	As	Se	Br	Kr																												
Rb	Sr	Y	Zr	Nb	Mo	Tc	Ru	Rh	Pd	Ag	Cd	In	Sn	Sb	Te	I	Xe																												
Cs	Ba	Lu	Hf	Ta	W	Re	Os	Ir	Pt	Au	Hg	Tl	Pb	Bi	Po	At	Rn																												
Fr	Ra	Lr	Rf	Db	Sg	Bh	Hs	Mt	Ds	Rg	Uub	Uut	Uuq	Uup	Uuh	Uus	Uuo																												
<table border="1"> <tr> <td>La</td><td>Ce</td><td>Pr</td><td>Nd</td><td>Pm</td><td>Sm</td><td>Eu</td><td>Gd</td><td>Tb</td><td>Dy</td><td>Ho</td><td>Er</td><td>Tm</td><td>Yb</td> </tr> <tr> <td>Ac</td><td>Th</td><td>Pa</td><td>U</td><td>Np</td><td>Pu</td><td>Am</td><td>Cm</td><td>Bk</td><td>Cf</td><td>Es</td><td>Fm</td><td>Md</td><td>No</td> </tr> </table>																		La	Ce	Pr	Nd	Pm	Sm	Eu	Gd	Tb	Dy	Ho	Er	Tm	Yb	Ac	Th	Pa	U	Np	Pu	Am	Cm	Bk	Cf	Es	Fm	Md	No
La	Ce	Pr	Nd	Pm	Sm	Eu	Gd	Tb	Dy	Ho	Er	Tm	Yb																																
Ac	Th	Pa	U	Np	Pu	Am	Cm	Bk	Cf	Es	Fm	Md	No																																

Figure 1. The locations of metal cations (green) that can form hydroxides.

and structure of LHs intercalated with guest anions are demonstrated first. Then, considering the rapid development in the field of preparing LHs intercalated with anions, we included the typical and newly appeared synthesis methods of LHs intercalated with anions and discussed not only the potential effect of external reaction parameters on the intercalation or non-intercalation of anions into LHs but also the advantages and disadvantages of each synthesis method. Besides, the analytical characterization techniques for the intercalated anions and the intercalation mechanism are discussed. It is expected that this review can not only provide some insight into this knowledge for researchers but also help researchers to realize the potential problems and identify the future research directions for the fundamental understanding of LHs intercalated with guest anions.

2. Chemical Composition, Structure, and Maintenance of Electrical Neutrality of LHs Intercalated with Guest Anions

Metal hydroxide is a basic metal compound made of metal cations and hydroxide anions. The locations of metal cations that can form hydroxides are illustrated in the Periodic Table (Figure 1),^[22]

and having such a library of usable metal cations enables the preparation of a range of hydroxides with a versatile structural composition. Not all hydroxides have layered structures, but many hydroxides do, such as alkaline earth hydroxides, transition metal hydroxides, and LDH. Mg(OH)₂ (Brucite), which was first described in 1824 by François Sulpice Beudant,^[23] is one of the most typical LHs. As shown in Figure 2a, in Brucite's structure, infinite 2D layers are built by six hydroxide anions edges coordinating with the Mg²⁺ centered octahedron, and these layers with neutralized charges are held together by van der Waals forces. Other LHs possessing brucite-like arrangements are Ca(OH)₂, Mn(OH)₂, Fe(OH)₂, Co(OH)₂, Ni(OH)₂, Zn(OH)₂, Cu(OH)₂ and Cd(OH)₂.^[24] Table 1 shows the crystallographic descriptions of these LHs with brucite-like structures, and it is easy to find that these LHs possess very similar structures except Cu(OH)₂. The structure of Cu(OH)₂ (Figure 2b) is 2D and consists of two Cu–OH sheets. Cu²⁺ is bonded to five O²⁻ atoms to form a mixture of edge and corner-sharing CuO₃ square pyramids and there is a spread of Cu–O bond distances ranging from 1.97–2.30 Å.^[21] Such a layered structure enables these LHs to accommodate various anions between interlayers to form LHs intercalated with guest anions, providing a new way for creating new materials and extending the application of such materials to more fields.

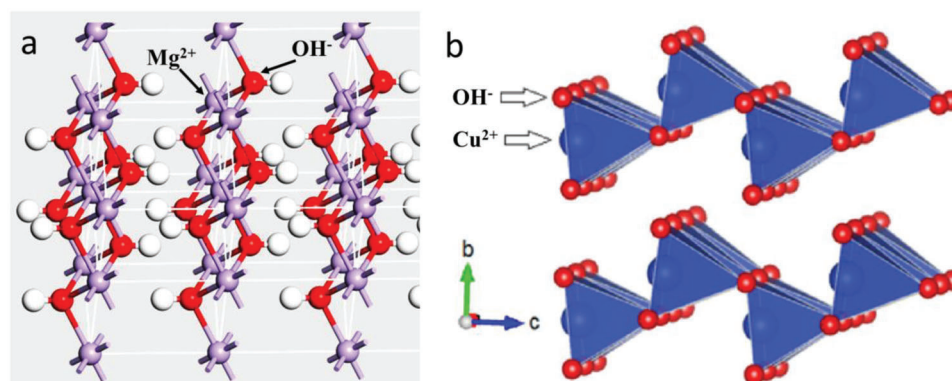


Figure 2. The atomic structures of a) Mg(OH)₂ (Brucite) and b) Cu(OH)₂. b) Reproduced with permission.^[12] Copyright 2021, Elsevier.

Table 1. The crystallographic descriptions of some LHs with brucite-like structure.

Material	Space group	Lattice constants						Unit cell volume [Å ³]	Ref.
		a [Å]	b [Å]	c [Å]	α [°]	β [°]	γ [°]		
Mg(OH) ₂	P-3m1	3.142	3.142	4.766	90	90	120	40.7	[13]
Ca(OH) ₂	P-3m1	3.5862	3.5862	4.8801	90	90	120	54.4	[14]
Mn(OH) ₂	P-3m1	3.25	3.25	4.48	90	90	120	40.98	[15]
Fe(OH) ₂	P-3m1	3.258	3.258	4.605	90	90	120	42.331	[16]
Co(OH) ₂	P-3m1	3.173	3.173	4.64	90	90	120	40.5	[17]
Ni(OH) ₂	P-3m1	3.114	3.114	4.617	90	90	120	38.8	[18]
Zn(OH) ₂	P-3m1	3.194	3.194	4.714	90	90	120	41.648	[19]
Cd(OH) ₂	P-3m1	3.52	3.52	4.64	90	90	120	49.69	[20]
Cu(OH) ₂	Cmc2 ₁	2.97	10.45	5.61	90	90	90	170.04	[21]

Discussing the structure, composition, and maintenance of electrical neutrality of LHs intercalated with guest anions is essential for understanding the intercalation mechanism of guest anions, and then both optimizing the synthesis conditions of LHs intercalated with guest anions and realizing the custom synthesis of LHs with the desired attributes. In this part, we will restrict the focus to LHs intercalated with guest anions based on the modification of the above-mentioned brucite-like structure, including namely the alkaline earth hydroxides intercalated with guest anions, transition metal hydroxides intercalated with guest anions and LDH intercalated with guest anions because these materials are attracting an increasing level of attention in a wide range of applications due to their structural/compositional versatility and unique physicochemical properties.^[1c,2-6]

2.1. The Alkaline Earth Hydroxides Intercalated With Guest Anions and Transition Metal Hydroxides Intercalated With Guest Anions

The alkaline earth hydroxides intercalated with guest anions and transition metal hydroxides intercalated with guest anions can

be regarded as the modification of the above-mentioned brucite-like structure by substitution of part of the hydroxide groups by appropriate anions or water molecules. These LHs intercalated with guest anions have a crystal structure with a general formula of $[M^{2+}(\text{OH})_{2-y}]^{y+}[\text{A}^{n-}]_{y/n}^{y-} \cdot m\text{H}_2\text{O}$, respectively, where M^{2+} is a divalent cation (e.g., Ni^{2+} , Co^{2+} , Fe^{2+} , Mn^{2+} , Mg^{2+} , Ca^{2+} , Cu^{2+} , Zn^{2+} , Cd^{2+} , etc.) and A^{n-} is an interlayer anion (e.g., NO_3^- , CO_3^{2-} , Cl^- , SO_4^{2-} , acetate, lactate, dodecyl sulfate, and oleate, etc.). **Table 2** presents the crystallographic descriptions of some typical alkaline earth hydroxides intercalated with guest anions and transition metal hydroxides intercalated with guest anions. Comparing the crystallographic descriptions of LHs with and without intercalated anions, we found that the intercalation of anions causes an increase in interlayer spacing, and the amount or type of intercalated anions can cause different changes in the structure of LHs. To better understand the structure of the above LHs intercalated with anions, their crystal structures in polyhedral representation are presented and compared. As we can see in **Figure 3**, their structures vary from one material to the other. To be specific, in the structure of NiOHCl , $\text{Cu}_2(\text{OH})_3\text{NO}_3$, and $\text{Cu}_4(\text{OH})_6\text{SO}_4 \cdot 2\text{H}_2\text{O}$, the layers are built of M (M = metal atom)

Table 2. The crystallographic descriptions of some typical alkaline earth hydroxides intercalated with guest anions and transition metal hydroxides intercalated with guest anions.

Material	Space group	Lattice constants						Unit cell volume [Å ³]	Ref.
		a [Å]	b [Å]	c [Å]	α [°]	β [°]	γ [°]		
Mg ₂ (OH) ₃ NO ₃	R-3m	3.13	3.13	6.94	90	90	120	58.9	[25]
Co ₂ (OH) ₃ NO ₃	P1211	5.5	6.3	6.94	90	90	90	240.5	[26]
Co _{1.176} (OH) _{2.004} Cl _{0.348} (H ₂ O) _{0.454}	R-3m	3.1439	3.1439	24.058	90	90	120	205.934	[27]
Ni ₂ (OH) ₃ NO ₃	R-3m	3.12	3.12	6.9	90	90	120	58.3	[28]
Zn ₅ (OH) ₈ Cl ₂ ·H ₂ O	R-3m	6.34	6.34	23.646	90	90	120	823.439	[29]
Zn ₅ (OH) ₈ (NO ₃) ₂ ·2H ₂ O	C12/m1	19.48	6.238	5.517	90	93.28	90	669.3	[30]
Zn ₄ (OH) ₆ SO ₄ ·4H ₂ O	P-3	8.33	8.33	10.54	90	90	120	633.375	[31]
Zn ₅ (OH) ₈ (NO ₃) ₂	C12/m1	5.39	6.28	17.92	90	91.14	90	606.9	[32]
Zn ₃ (OH) ₄ (NO ₃) ₂	P121/c1	7.04	9.63	11.22	90	100.75	90	747.3	[33]
Cu ₂ (OH) ₃ NO ₃	P1211	5.61	6.01	6.93	90	94.48	90	470.6	[34]
Cu ₄ (OH) ₆ (SO ₄)·H ₂ O	P1c1	6.045	5.646	14.337	90	93.39	90	488.467	[35]
Cu ₃ (OH) ₅ NO ₃ ·2H ₂ O	Pcmm	5.83	6.775	21.711	90	90	90	857.547	[36]

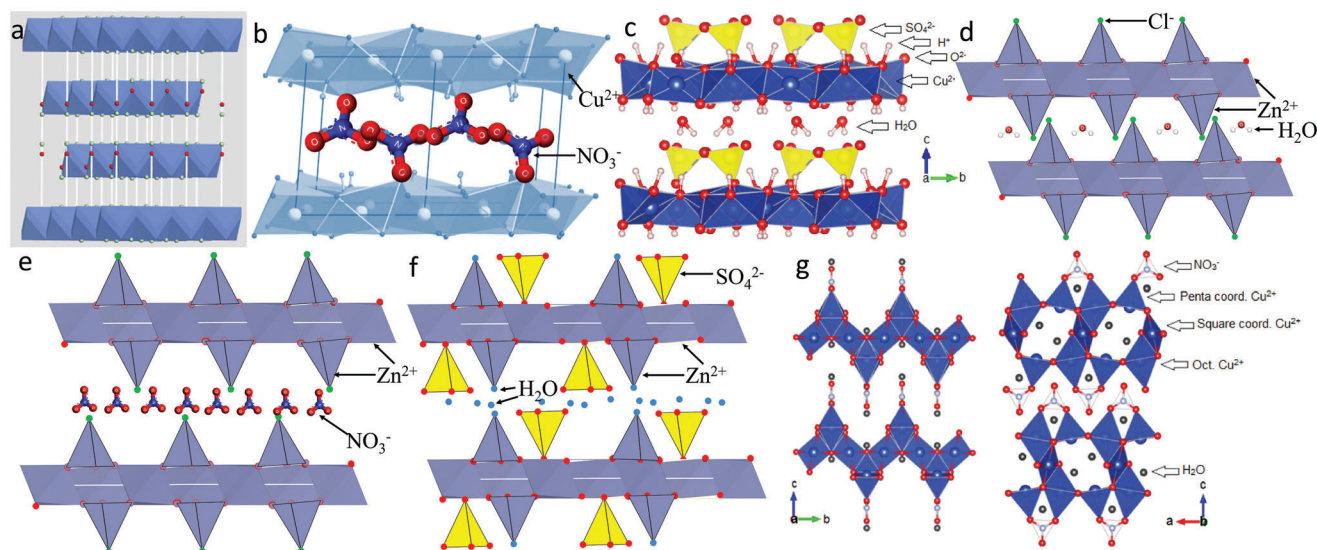


Figure 3. The atomic structures of a) NiOHCl, b) $\text{Cu}_2(\text{OH})_3\text{NO}_3$, c) $[\text{12}] \text{Cu}_4(\text{OH})_6\text{SO}_4 \cdot 2\text{H}_2\text{O}$, d) $\text{Zn}_5(\text{OH})_8\text{Cl}_2 \cdot \text{H}_2\text{O}$, e) $\text{Zn}_5(\text{OH})_8(\text{NO}_3)_2 \cdot 2\text{H}_2\text{O}$, f) $\text{Zn}_4(\text{OH})_6\text{SO}_4 \cdot 4\text{H}_2\text{O}$ and g) $[\text{12}] \text{Cu}_3(\text{OH})_5\text{NO}_3 \cdot 2\text{H}_2\text{O}$. c,g) Reproduced with permission.^[12] Copyright 2021, Elsevier.

octahedra coordinated to six OH^- groups and part of these six OH^- groups are replaced by intercalated anions. If the intercalation of water molecules takes place simultaneously, these intercalated water molecules are distributed along the basal distance in the interlayer space.^[37] Note that Cu octahedra in $\text{Cu}_2(\text{OH})_3\text{NO}_3$ and $\text{Cu}_4(\text{OH})_6\text{SO}_4 \cdot 2\text{H}_2\text{O}$ are Jahn-Teller distorted. In the structure of $\text{Zn}_5(\text{OH})_8\text{Cl}_2 \cdot \text{H}_2\text{O}$, there are two types of coordination environment of Zn species, namely Zn atom in octahedral or tetrahedral coordination. Octahedral Zn coordinates with six OH^- groups and tetrahedral Zn coordinates with three OH^- groups and one chloride in the apical site. One Zn vacant site is situated between the tetrahedral Zn sites located above and below the layers, with water molecules occupying the space between the layers.^[29] $\text{Zn}_5(\text{OH})_8(\text{NO}_3)_2 \cdot 2\text{H}_2\text{O}$ exhibits a structure akin to $\text{Zn}_5(\text{OH})_8\text{Cl}_2 \cdot \text{H}_2\text{O}$, with one key difference: in the former, water molecules occupy the apex position of the tetrahedral Zn instead of NO_3^- anions. As a result, the NO_3^- anions are distributed between the layers, allowing for easier substitution with other anionic species.^[30] The structure of $\text{Zn}_4(\text{OH})_6\text{SO}_4 \cdot 4\text{H}_2\text{O}$ is similar to that of $\text{Zn}_5(\text{OH})_8(\text{NO}_3)_2 \cdot 2\text{H}_2\text{O}$ except that the SO_4^{2-} anion is coordinated to an octahedral site that is previously occupied by OH^- .^[38] $\text{Cu}_3(\text{OH})_5\text{NO}_3 \cdot 2\text{H}_2\text{O}$ has a relatively complex structure that can be represented along two distinct structural axes. The layers are composed of Cu^{2+} ions that are coordinated in square planar, square pyramidal, and octahedral coordination polyhedra. NO_3^- anions alternate between pointing toward both sides of the layers and are linked through O–N–O bridges to one Cu^{2+} ion with a pentacoordinated geometry and another with a hexacoordinated geometry.^[36] Based on the above discussion, the alkaline earth hydroxides intercalated with guest anions and transition metal hydroxides intercalated with guest anions can be divided into several types according to the possibilities of arranging the metal cations, hydroxide groups, intercalated anions, and water molecules. To be specific, type I structure consists of metal species coordinated solely in an octahedral arrangement to form the main layers, with the intercalated anions

directly coordinated to the metal species. The typical LHs intercalated with anions belonging to type I structure include NiOHCl, $\text{Cu}_2(\text{OH})_2(\text{NO}_3)_2$, $\text{Cu}_2(\text{OH})_3\text{NO}_3$, $\text{Mg}_2(\text{OH})_3\text{NO}_3$, $\text{Ni}_2(\text{OH})_3\text{NO}_3$, $\text{Zn}_2(\text{OH})_2(\text{NO}_3)_2 \cdot 2\text{H}_2\text{O}$ and $\text{Cu}_4(\text{OH})_6\text{SO}_4 \cdot 2\text{H}_2\text{O}$. Type II structures also possess main octahedral layers, but some of the metal species are displaced to tetrahedral sites located on both sides of the main layer. The base of the tetrahedra shares OH^- groups with the octahedral layer and the apex of such tetrahedral site is occupied by the intercalated anions. Examples of Type II structures are anhydrous $\text{Zn}_5(\text{OH})_8(\text{NO}_3)_2$ and $\text{Zn}_5(\text{OH})_8\text{Cl}_2 \cdot \text{H}_2\text{O}$. The structure of type III is similar to that of type II, but instead of having the intercalated anions coordinated with the apex of the tetrahedral metal species, water molecules occupy the site and the intercalated anions are allocated between the layers or connected with the octahedral metal species. $\text{Zn}_5(\text{OH})_8(\text{NO}_3)_2 \cdot 2\text{H}_2\text{O}$ and $\text{Zn}_4(\text{OH})_6\text{SO}_4 \cdot 4\text{H}_2\text{O}$ are LHs intercalated with anions that belong to type III. The structure of type IV refers to LHs intercalated with anions, such as $\text{Cu}_3(\text{OH})_5\text{NO}_3 \cdot 2\text{H}_2\text{O}$, possessing a coordination environment other than tetrahedral and octahedral coordination. Although the above-mentioned alkaline earth hydroxides intercalated with guest anions and transition metal hydroxides intercalated with guest anions contain only one type of metal cation, LHs intercalated with guest anions composed of two or three different divalent cations can also be found (type V).^[39] In this case, the difference in cation radii should not exceed 0.5×10^{-2} nm, but recent studies have demonstrated the successful preparation of such hydroxides with metal cations such as Cd^{2+} and Cu^{2+} , which have a radius difference of 2.2×10^{-2} nm.^[40]

Although the structure of LHs intercalated with anions varies from one material to the other, there is one thing in common, namely the maintenance of electrical neutrality of LHs intercalated with guest anions depending on the balance between the positively charged $\text{M}(\text{OH})_{2-x}$ layers and the intercalated anions. However, the mechanism for the incorporation of the intercalated anions into the matrix of LHs is still under debate.

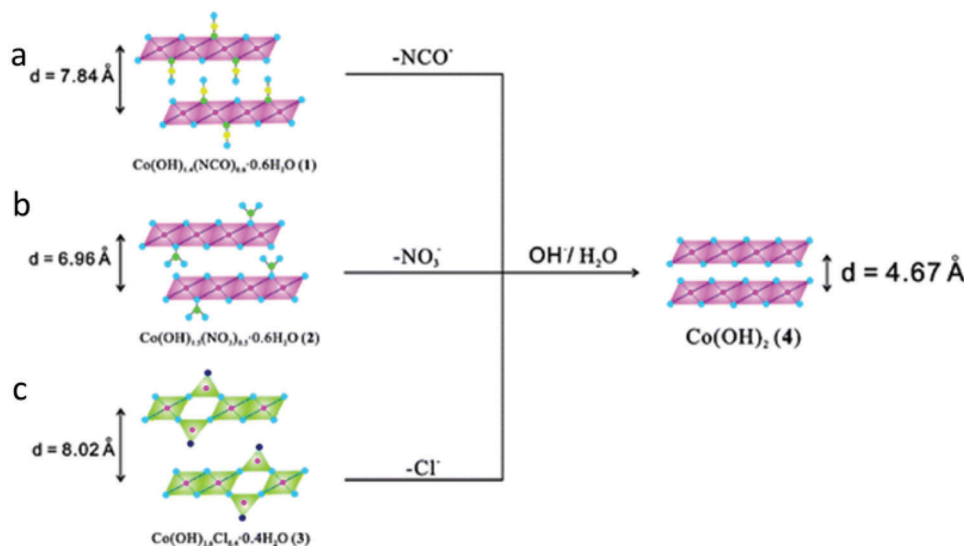


Figure 4. Schematic representations of several possible structure models of α - $\text{Co}(\text{OH})_2$. a) $\text{Co}(\text{OH})_{1.4}(\text{NCO})_{0.6} \cdot 0.6\text{H}_2\text{O}$; b) $\text{Co}(\text{OH})_{1.5}(\text{NO}_3)_{0.5} \cdot 0.6\text{H}_2\text{O}$; c) $\text{Co}(\text{OH})_{1.6}\text{Cl}_{0.4} \cdot 0.4\text{H}_2\text{O}$. Reproduced with permission.^[41] Copyright 2008, Royal Society of Chemistry.

Taking cobalt hydroxide intercalated with anions as an example, so far, several debated theories attempt to explain the mechanism of maintaining electrical neutrality. The first model suggests a partial substitution of the Co^{2+} by Co^{3+} ions in the octahedral layers,^[42] making the compound analogous to LDHs. Obviously, the increased valence of Co species is the key to compensating for the negative charge of the intercalated anions, and the reliability of such theory can be verified by evaluating the valence of Co species. As shown in **Figure 4a,b**, the second model is the simple partial replacement of hydroxide by the intercalated anions to restore electrical neutrality.^[41] This particular model not only anticipates that the ultimate hydroxide product will exhibit its distinctive pink color due to the exclusive presence of octahedral Co^{2+} ions, but it also predicts a comparatively smaller interlayer spacing because the intercalated anions occupy a specific site that is coordinated with the Co^{2+} ions, rather than locating in the space between the interlayers. As shown in **Figure 4c**, the third model predicts a characteristic green color due to the existence of additional Co^{2+} ions on interstitial, tetrahedral-symmetry sites between interlayers.^[41] To be specific, some Co^{2+} ions are tetrahedrally bonded to hydroxyl ions in neighboring octahedra and the intercalated anions exist between the layers. In this case, $\text{Co}(\text{OH})_2$ intercalated with anions thus possesses a larger interlayer spacing (usually > 0.7 nm, dependent on intercalated anions) than that of the $\text{Co}(\text{OH})_2$ without intercalated anions (0.46 nm). Although the above three models have appeared in the literature, most reports utilized the existence of additional tetrahedrally bonded Co^{2+} ions to explain the possible structure of α - $\text{Co}(\text{OH})_2$ and the mechanism of maintaining electrical neutrality. In our opinion, the above-mentioned different models apply to different LHs intercalated with anions, and the intercalation mechanism of anions for one specific system is strongly related to the type or amount of the intercalated anions. We believe that, with the help of appropriate characterization techniques, the intercalation mechanism of anions into LHs prepared in one synthesis system can be fully understood. One typical example

is that Ma et al. synthesized $\text{Co}(\text{OH})_2$ intercalated with Cl^- via heating a mixture of deionized water and ethanol (9:1) containing $\text{CoCl}_2 \cdot 6\text{H}_2\text{O}$, NaCl, and hexamethylenetetramine at about 90°C under magnetic stirring.^[27] The authors employed X-ray absorption spectroscopy to demonstrate the exclusive presence of Co^{2+} in the obtained hydroxides, excluding the possibility of the existence of Co^{3+} in the product. Meanwhile, the XRD result in their study suggested the increased interlayer spacing of the obtained hydroxides, which is contradicted by the model that the simple partial substitution of hydroxyl by other anions could result in the presence of exclusively Co^{2+} octahedra and the relatively small interlayer spacing. Based on the above analysis, the authors believed that maintaining charge neutrality of $\text{Co}(\text{OH})_2$ intercalated with Cl^- depends on the existence of tetrahedrally bonded Co^{2+} cations, of which the rationality is also supported by the green color of their product and the existence of 4-coordinated Co^{2+} tetrahedra evidenced by X-ray absorption spectroscopy and UV-vis spectroscopy results.

2.2. Layered Double Hydroxides Intercalated With Guest Anions

The structure of LDHs intercalated with guest anions can be regarded as the brucite structure undergoing compositional changes with minor structural modifications, of which a trivalent metal cation (M^{3+}) isomorphically replaces part of the Mg^{2+} . The general formula of hydroxalite-type LDHs is $[\text{M}^{2+}_{1-x}\text{M}^{3+}_x(\text{OH})_2]^{x+}[\text{A}^{n-}_{x/n}]^{x-} \cdot m\text{H}_2\text{O}$, in which M^{2+} and M^{3+} are metallic divalent and trivalent cations, respectively, and A^{n-} are the interlayered anions.^[51] The degree of positive charge in the framework is determined by the ratio of M^{2+}_{1-x} to M^{3+}_x cations, with a low $\text{M}^{2+}:\text{M}^{3+}$ ratio resulting in highly positively charged layers. LDH phases that are purely composed can be found within the x range of 0.2 to 0.33.^[52] If x is > 0.337 , the boehmite ($-\text{AlOOH}$) structure will form, whereas for x between 0.105 and 0.201, the hydromagnesite ($4\text{MgCO}_3 \cdot \text{Mg}(\text{OH})_2 \cdot 4\text{H}_2\text{O}$) structure

Figure 5. Locations in the Periodic Table of cations, which have been reported as constituents of the layers in LDHs. Blue, divalent cations; green, trivalent cations; red, monovalent cations; yellow, tetravalent cations.

will form. For values of x below 0.105, a combination of hydro-magnesite and $M(OH)_2$ will be formed. The corresponding locations of metal cations, which have been reported to be used to prepare LDHs, in the Periodic Table are illustrated in **Figure 5**.^[22a] Several empirical studies have attempted to determine the criteria for identifying metal ions that can form LDHs. The most commonly cited “rule” is that the ionic radius of the metal cation being incorporated into LDH layers should be similar to that of Mg^{2+} (0.720 Å). However, there are still some exceptions. For example, Ca^{2+} and Cd^{2+} with significantly larger ionic radii (1.000 Å and 0.950 Å, respectively) than that of Mg^{2+} are incorporated into LDH layers, resulting in relatively stable structures.^[53] **Table 3** presents the crystallographic descriptions of some typical LDHs. Unlike the various structures of the alkaline earth hydroxides intercalated with guest anions and transition metal hydroxides intercalated with guest anions, different LDHs have similar structures and crystallographic descriptions. The crystal structure of LDHs is schematically illustrated in **Figure 6**. It can be seen that LDHs consist of a divalent metal cation located in the center of oxygen octahedra and 2D infinite layers formed by the edge-sharing of octahedra. The brucite-type layers are arranged in a stacked manner and are weakly bonded together through the hydrogen atoms.^[54] The interlamellar domain must be filled with a sufficient number of anions, typically in a hydrated state, to maintain electrical neutrality resulting from partial substitution of isomorphous trivalent metal cations for divalent ones.^[55] In other words, the intercalation of anions for LDHs is driven by the

$M-OH$ layers’ positive charge generated by partial substitution of the M^{2+} by M^{3+} ions,^[56] which differs from the intercalation of anions for LHS intercalated with anions in the last part caused by the amount decrease of OH^- groups.

In the early stage of studies on LDHs, the introduced metal species were mainly divalent and trivalent. Recently, the library of host slabs has been further expanded to incorporate monovalent and tetravalent metal cations.^[57] Besides, LDHs are not limited to binary combinations of metal cations, while ternary, quaternary, and multicomponent LDHs can also be synthesized.^[57b,58] As for the intercalated anions between adjacent layers, apart from the typical inorganic anions (commonly NO_3^- , SO_4^{2-} , CO_3^{2-} , Cl^- , etc.), researchers have successfully applied many corresponding guest organic anions to replace the original anions of LDHs through a two-step synthesis process (co-precipitation and anionic exchange) or one-step synthesis process (i.e., direct co-precipitation method).^[59] The intercalated anions are connected with the $M-OH$ layers via forming complex interactions such as hydrogen bonding with the hydroxyl groups of the host layer as well as electrostatic interactions.

Note that some LHS intercalated with anions, which contain metallic divalent and trivalent cations, possess a similar structure to LDHs, but they should be classified as transition metal hydroxides intercalated with guest anions. One typical example is Jamborite, which was found to possess an optimal composition of $Ni^{2+}_{1-x}Co^{3+}_x(OH)_{2-x}(SO_4)_x \cdot nH_2O$.^[60] In the examined sample, the value of “ x ” was ≈ 0.1 with $n \leq (1-x)$. The X-ray powder diffraction

Table 3. The crystallographic descriptions of some typical LDHs.

Material	Space group	Lattice constants						Unit cell volume [Å ³]	Ref.
		a [Å]	b [Å]	c [Å]	α [°]	β [°]	γ [°]		
$Mg_4Al_2(OH)_{12}Cl_2 \cdot 2H_2O$	P63/mcm	5.268	5.268	15.3	90	90	120	367.6	[43]
$Mg_6Fe_2(OH)_{16}CO_3 \cdot 4H_2O$	P63/mcm	21.57	21.57	15.61	90	90	120	6287.7	[44]
$Zn_4Al_2(OH)_{12}(CO_3) \cdot 3H_2O$	P63/mmc	3.07	3.07	15.11	90	90	120	123.56	[45]
$Zn_{0.67}Al_{0.33}(OH)_2(NO_3)_{0.33} \cdot 0.85H_2O$	R-3mh	3.08	3.08	26.7	90	90	120	219	[46]
$Mg_6Cr_2CO_3(OH)_{16} \cdot 4H_2O$	R-3mh	3.1	3.1	23.5	90	90	120	195	[47]
$Ni_4Al_2(OH)_{12}CO_3 \cdot 3H_2O$	R-3mh	3.03	3.03	22.85	90	90	120	182	[48]
$Ni_7Fe_3(OH)_{19.8}(CO_3)_{1.6} \cdot 6.1H_2O$	R-3mh	3.08	3.08	23.07	90	90	120	189.5	[49]

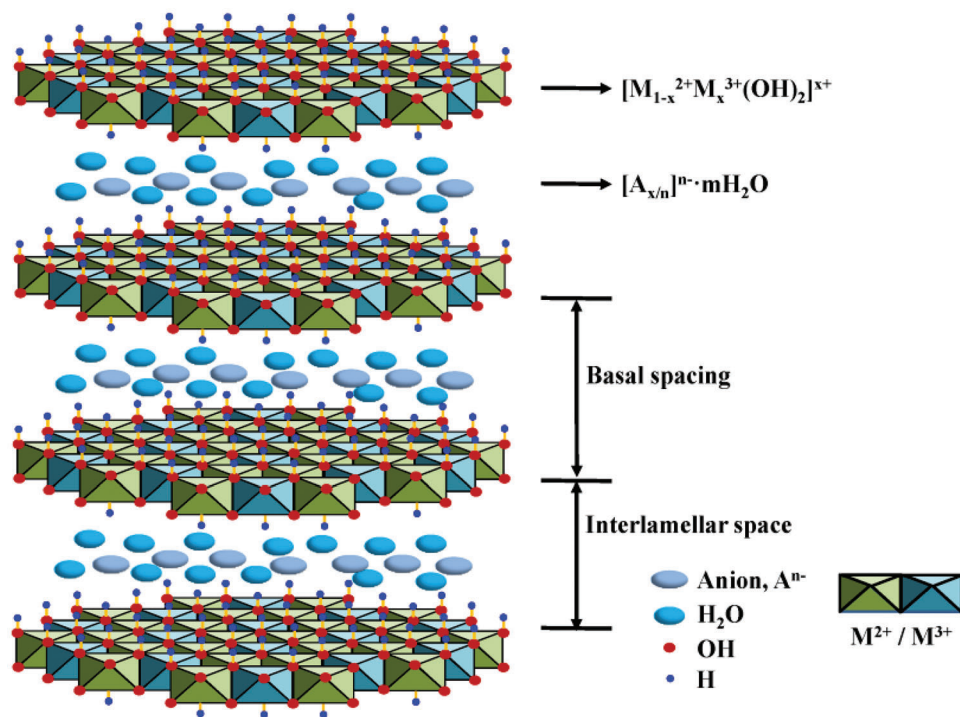


Figure 6. Structural representation of the crystal structure of hydrotalcite-type LDHs. Reproduced with permission.^[50] Copyright 2020, MDPI.

pattern indicated a hexagonal unit cell with dimensions $a = b = 3.068 \text{ \AA}$ and $c = 23.298 \text{ \AA}$. Although this mineral bears a strong resemblance to the hydrotalcite family (a type of LDHs), the authors claimed that “structural investigation shows that Jamborite lies outside the hydrotalcite supergroup”, which is backed by another publication^[61] and the following evidence: 1, the brucite-like layers of Jamborite consist of a high concentration of M^{2+} (with an M^{2+}/M^{3+} ratio close to 9:1), which is higher than that of LDHs; 2, sulfate tetrahedra are attached to the layers, partially displacing OH^- anions, rather than being intercalated between the layers as in LDHs; 3, one sulfate requires only one M^{3+} cation to balance its charge in Jamborite, whereas the M^{3+} to sulfate ratio in LDHs is 2:1; 4, based on the classification of the transition metal hydroxides intercalated with guest anions with the formula $[\text{M}^{2+}(\text{OH})_{2-y}]^{y+}[\text{A}^{n-}_{y/n}]^{y-} \cdot m\text{H}_2\text{O}$, where the compounds are deficient in OH^- .

3. The Preparation Methods of LHs Intercalated With Guest Anions

Various synthesis methods have been developed to prepare LHs intercalated with guest anions for meeting academic and industrial demands, and these synthesis methods can generally be classified into two categories: the top-down approach and the bottom-up approach.^[62] The top-down approach involves decreasing the thickness of bulk (or micro) LHs intercalated with guest anions via enlarging the interlayer distance and weakening the interlayer forces, while the bottom-up approach starts from suitably designed molecular precursors to build up 2D networks of LHs intercalated with guest anions connected by chemical bonds. Considering that the top-down approach may not involve the interca-

lation of guest anions, in this part, we mainly focus on the studies involving the bottom-up approach, especially literature presenting the factors that influence the intercalation of guest anions.

3.1. Conventional Hydrothermal/Solvothermal Synthesis

One of the most widely used preparation methods for hydroxides is the conventional hydrothermal/solvothermal synthesis, in which metal salt and precipitators are mingled in solvent (water or organic solvents or the mixture) and react under the condition of high temperature (80–300 °C) and increased pressure in an airtight vessel.^[63] When exposed to high temperature and high pressure, the used solvent undergoes changes in dielectric constant, viscosity, and dissociation constant.^[64] These changes promote electrostatic interactions and expedite crystal ripening. It has been widely demonstrated that the application of this treatment leads to products with a higher degree of crystallinity and larger crystals compared to those produced through the conventional precipitation method using alkaline solutions.^[65] Recently, hydrothermal/solvothermal treatment has been regarded as an efficient method for the preparation of LHs intercalated with guest anions, of which different reaction parameters, such as solvent, reaction temperature, and reagent concentration, can be tuned. For example, Gao et al. synthesized $\alpha\text{-Ni}(\text{OH})_2$ intercalated with NO_3^- via hydrothermal treating a mixture of oleylamine and ethanol containing $\text{Ni}(\text{NO}_3)_2 \cdot 6\text{H}_2\text{O}$ at 180 °C for 15 h in a Teflon-lined autoclave. Interestingly, the same synthesis procedure except that the ethanol was replaced by distilled water resulted in the formation of $\beta\text{-Ni}(\text{OH})_2$ without intercalated NO_3^- .^[66] Although the authors did not mention the reason for the presence

and absence of intercalated NO_3^- in the structure of $\text{Ni}(\text{OH})_2$, it is obvious that water plays a key role in determining the successful intercalation of NO_3^- . Note that the amount of water is not necessarily the more the better for promoting the intercalation of anions, which is supported by the case of synthesizing NiCo-LDH in the mixed solvent of 1-methyl-2-pyrrolidone (NMP) and deionized water through a hydrothermal process (180 °C for 6 h), in which the increased volume ratio of deionized water and NMP leads to the failure in the intercalation of NO_3^- anions into the structure of LHs.^[67] The reaction temperature is another variable that affects the intercalation of anions. The first example is that 80 mL aqueous solution containing $\text{Ni}(\text{NO}_3)_2 \cdot 6\text{H}_2\text{O}$ and urea, which was placed in a Teflon-lined autoclave with a 100 mL capacity, was held at different temperatures for 2 h, and the products formed at 120/150/180 °C and 200 °C are recognized as $\text{Ni}(\text{OH})_2$ with and without the intercalated anions, respectively.^[68] The second example is that the low hydrothermal temperature results in the generation of $\text{Mg}(\text{OH})_2$, while $\text{Mg}(\text{OH})_2$ intercalated with SO_4^{2-} tends to form at the high hydrothermal temperature.^[69] Based on the discussion of these two examples, we infer that the influence of reaction temperature on controlling the intercalation of anions is not governed by a consistent pattern and varies from one synthesis scheme to the other. Aside from solvent and reaction temperature, tuning reagent concentration also significantly contributes to the controllable intercalation of anions. One typical example is that Li et al.^[70] prepared α -Co(OH)₂ intercalated with Cl^- by dissolving $\text{CoCl}_2 \cdot 6\text{H}_2\text{O}$ (20 mM) and hexamine in a mixture of deionized water and ethanol and then hydrothermal treatment of such mixture at 90 °C for 1 h, and preventing the intercalation of Cl^- was realized by performing a similar synthetic procedure to α -Co(OH)₂ intercalated with Cl^- except decreasing the concentration of $\text{CoCl}_2 \cdot 6\text{H}_2\text{O}$ to 5 mM. We think there is probably a competition between OH^- and Cl^- for coordinating with Co species, and the relative concentration ratio of these two types of ions is crucial in achieving successful intercalation of Cl^- . In summary, without a doubt, tuning reaction parameters, such as solvent, reaction temperature, and reagent concentration, can realize the controllable intercalation of anions. However, the effect of these parameters on the intercalation remains to be elucidated. Besides, although hydrothermal/solvothermal treatment represents an effective means of producing hydroxides with a high degree of crystallinity and large size, this route suffers from the following disadvantages: 1, the synthesis scheme varies from one system to the other, prohibiting a universal synthesis strategy; 2, this synthesis route has a relatively long reaction time, which is typically 6 to 24 h or more; 3, the employment of high reaction temperature and pressure means high energy consumption; 4, the elevated temperature, high pressure and the use of an airtight vessel limit the ability to carry out in situ characterization, increasing the difficulty of understanding the formation mechanism of LHs and making the hydrothermal/solvothermal method a “black box” technology.

3.2. Liquid Phase Precipitation Method Under Relatively Mild Conditions

Liquid phase precipitation synthesis under relatively mild conditions is another widely used preparation method for LHs, and it

is a precipitation process of metal ions driven by the increase of OH^- concentration. Such a synthesis route is very similar to conventional hydrothermal/solvothermal synthesis, except for lower reaction temperature (25–100 °C) and without using any container, which supports the pressure of the solvent vapor. Therefore, it is possible to adjust some similar reaction parameters to those in the above-mentioned hydrothermal/solvothermal route to influence the intercalation of anions into LHs. In the synthesis of Fe-doped $\text{Ni}(\text{OH})_2$, using $\text{Fe}_2(\text{SO}_4)_3 \cdot 4\text{H}_2\text{O}$ as Fe source leads to the generation of Fe^{3+} -doped α - $\text{Ni}(\text{OH})_2$ intercalated with SO_4^{2-} , while using $\text{FeSO}_4 \cdot 7\text{H}_2\text{O}$ as Fe source promotes the formation of Fe^{2+} -doped β - $\text{Ni}(\text{OH})_2$ without the intercalated SO_4^{2-} .^[71] Combining this experimental result with the discussion in part 2.2., we infer that the intercalation of SO_4^{2-} is for compensating for the negative charge of M–OH layers resulting from partial substitution of isomorphous trivalent metal cations for divalent ones. Actually, the intercalation of anions is not only affected by the valence state of the metal source but also by the counter anions in the metal salts. The example is that Yin et al. carried out three similar experimental schemes for the synthesis of $\text{Co}(\text{OH})_2$, and the only difference is using Co salts with different counter anions, namely CoCl_2 , $\text{Co}(\text{NO}_3)_2$, and $\text{Co}(\text{CH}_3\text{COO})_2$.^[72] Interestingly, α - $\text{Co}(\text{OH})_2$ phase with the intercalated Cl^- formed in the case of using CoCl_2 as Co source, while using $\text{Co}(\text{NO}_3)_2$ and $\text{Co}(\text{CH}_3\text{COO})_2$ as Co source resulted in the generation of β - $\text{Co}(\text{OH})_2$ without the intercalated anions, indicating the stronger intercalation ability of Cl^- than NO_3^- and CH_3COO^- under the same reaction condition. This difference could be due to the different competition ability of NO_3^- , CH_3COO^- and Cl^- with OH^- for coordinating with Co species, which bears resemblance to the above-mentioned influence of the relative concentration ratio of OH^- and counter anions on the competition between OH^- and Cl^- for coordinating with Co species. Note that the changed synthesis condition can also promote the successful intercalation of NO_3^- and CH_3COO^- into the structure of $\text{Co}(\text{OH})_2$. For instance, Hu et al.^[73] prepared $\text{Co}(\text{OH})_2$ intercalated with different anions by adding 10 g of polyethylene glycol into 50 mL of distilled water containing one of $\text{CoCl}_2 \cdot 6\text{H}_2\text{O}$, $\text{Co}(\text{NO}_3)_2 \cdot 6\text{H}_2\text{O}$, $\text{CoSO}_4 \cdot 7\text{H}_2\text{O}$ and $\text{Co}(\text{CH}_3\text{COO})_2 \cdot 4\text{H}_2\text{O}$ under vigorous stirring, and the resulting mixture was then aged for 12 h at room temperature. One key factor for the successful intercalation of different anions into the structure of $\text{Co}(\text{OH})_2$ is to adjust the pH of the solution to ≈ 9 using ammonia solution, which is different from the synthesis route of Yin et al.,^[72] as adjusting the pH of the reaction solution was not mentioned in this study. Actually, the key role of tuning pH in promoting the successful intercalation of anions into the structure of LHs has been demonstrated by many studies. For example, Delmas et al.^[74] found that the low (10) and high (13) pH corresponds to the formation of $\text{Ni}(\text{OH})_2$ with and without intercalated anion, respectively, while Morse et al.^[75] realized tuning the intercalation amount of Cl^- into the structure of $\text{Co}(\text{OH})_2$ via changing the concentration of the alkaline solution. Adjusting pH of the reaction solution means changing the concentration of OH^- , and then represents altering the competition ability of OH^- with the intercalated anions for coordinating with metal cations, which is consistent with the above statement that the relative concentration ratio of OH^- and counter anions affects the competition ability of these two types of anions for intercalation into the structure of LHs. Such presumption is supported

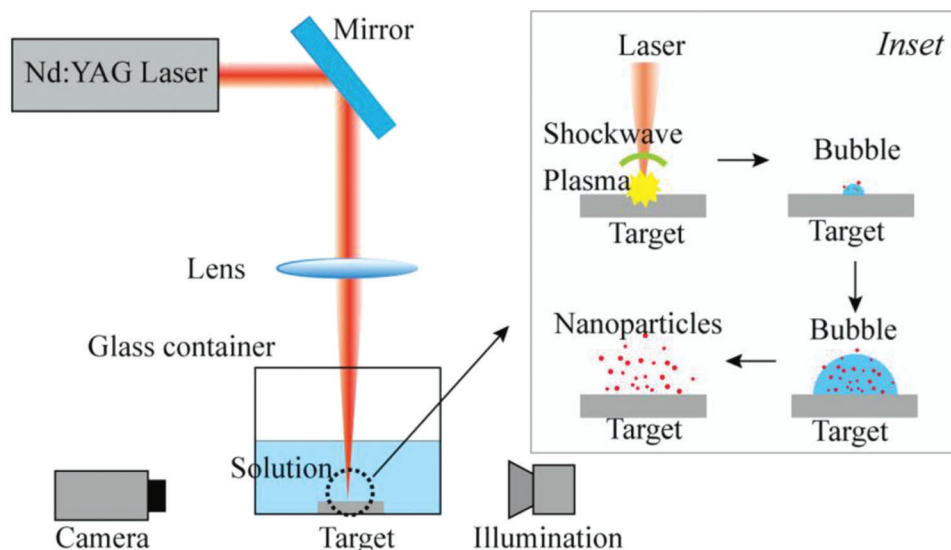


Figure 7. Schematic diagrams of experimental setup and PLAL process. Reproduced with permission.^[77] Copyright 2019, AIP Publishing.

by some reports that increasing the concentration of counter anions while keeping the concentration of OH^- constant can promote the successful intercalation of counter anions.^[76] It should be noted that liquid phase precipitation methods under relatively mild conditions differ between systems, making it difficult to develop a universal synthesis method.

3.3. Liquid Phase Synthesis With the Assistance of Pulsed-Laser Ablation, Microwave, Electrodeposition, etc

As shown by the schematic in **Figure 7**,^[77] the production of nanostructures using pulsed-laser ablation in liquid (PLAL) involves using a laser pulse to eject material from a solid target that is submerged in liquid.^[78] A typical example is that Müller et al.^[11e] synthesized NiFe-LDH via PLAL. Typically, suspensions of 0.5 g iron powder were stirred in 10 mL aqueous nickel salt solutions ($\text{Ni}(\text{NO}_3)_2 \cdot 6\text{H}_2\text{O}$, $\text{NiCl}_2 \cdot 6\text{H}_2\text{O}$ and $\text{NiSO}_4 \cdot 6\text{H}_2\text{O}$) using a magnetic stirrer in a 30 mL glass beaker at room temperature in ambient air. A pulsed laser beam was focused 0.5 mm below the surface of the liquid with a 100 mm focal length plano-convex quartz lens. Each sample was irradiated for 60 min. The successful synthesis of NiFe-LDH intercalated with different anions (Cl^- , NO_3^- and SO_4^{2-}) indicates that PLAL is an efficient method for preparing LHs intercalated with anions, and the success of this process depends on several factors, including the intensity and duration of the laser pulse, the properties of the liquid medium, and the shape and size of the target material. Additionally, the focusing conditions of the laser beam can also affect the efficiency and quality of the resulting nanostructures. PLAL can be employed to produce not only LDH but also monometallic LHs, and the example is that $\text{Mg}(\text{OH})_2$ nanostructures exhibiting wormhole-, tube-, rod- or platelet-like morphologies were prepared by pulsed laser ablation of an Mg plate target immersed in deionized water.^[79] By comparing the synthesis processes of the above NiFe-LDH and $\text{Mg}(\text{OH})_2$, it is easy to find that the presence of other metal ions in the liquid phase is the determining

factor for the synthesis of monometallic or multimetallic LHs. In our opinion, PLAL is a similar synthesis route to the above-mentioned liquid phase precipitation methods under relatively mild conditions, with the difference being that in PLAL, at least one kind of metal ion source is provided through pulsed laser ablation of a metal plate target. Therefore, it is reasonable to infer that tuning some reaction parameters, such as solvent or reagent concentration, can realize the controllable intercalation of anions. This is supported by the report by Koshizaki et al.^[80] that $\text{Zn}(\text{OH})_2$ intercalated with sodium dodecyl sulfate (SDS) was synthesized by pulsed-laser ablation of a metal Zn plate in an aqueous solution of SDS, while ZnO nanoparticles were formed when decreasing the concentration of SDS to 0.

The microwave-assisted technique is regarded as a novel method in the synthesis of LHs intercalated with anions and is a rapidly developing area of research. Actually, the microwave-assisted approach can be viewed as an improved method of hydrothermal/solvothermal synthesis and liquid phase precipitation methods under relatively mild conditions, because the only difference lies in the method of heating. Some authors have compared the effect of microwave heating and other heating methods on the quality of LHs, and it was found that, with the use of microwaves, $\text{Ni}_{1-x}\text{Zn}_{2x}(\text{OH})_2(\text{CH}_3\text{COO})_{2x} \cdot n\text{H}_2\text{O}$ grows two times faster compared to the conventional heating in a furnace.^[81] Furthermore, the degree of crystallinity of LHs was found to improve with increasing applied power. For instance, a synthesis using 600 W power yielded better crystals than those obtained at 200 W and 400 W.^[82] The microwave-assisted synthesis is known for its ease of use, speed, quietness, safety, controllability, and energy efficiency.^[83] Especially, this route can significantly decrease the synthesis time, and one example is that, in the report of Xiao et al. about the synthesis of $\text{Co}(\text{OH})_2$ intercalated with anions, the reaction solution was subjected to microwave radiation with an initial power of 400 W at a fixed temperature of 100 °C for only 10 min (≈ 4 min to reach 100 °C from room temperature).^[84] Note that the authors mentioned that $\alpha\text{-Co}(\text{OH})_2$ phase with the intercalated anions formed in the case of using CoCl_2 and CoSO_4

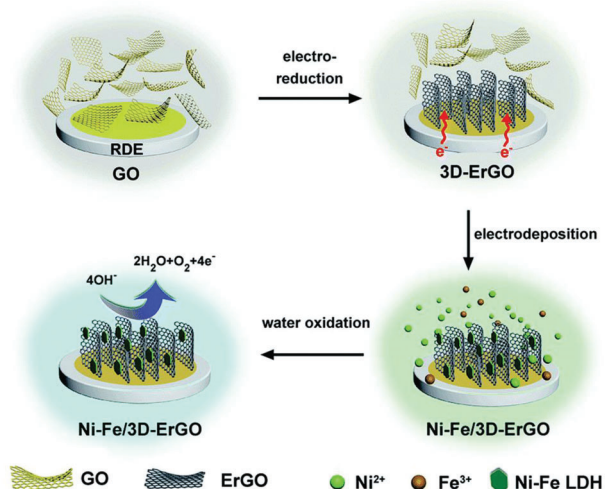


Figure 8. Fabrication and application of the NiFe-LDH/3D electrochemically reduced graphene oxide electrode. Reproduced with permission.^[85] Copyright 2015, Royal Society of Chemistry.

as Co source, while using $\text{Co}(\text{NO}_3)_2$ and $\text{Co}(\text{CH}_3\text{COO})_2$ as Co source resulted in the generation of $\beta\text{-Co}(\text{OH})_2$ without the intercalated anions, which is same with the finding of Yin et al. preparing $\text{Co}(\text{OH})_2$ using Co salts with different counter anions via liquid phase precipitation under relatively mild conditions,^[72] further confirming the similarity of microwave-assisted approach and the synthesis route in the part of 3.1/3.2.

In the electrodeposition process, one conductive material is typically used as a substrate for cathodic electroprecipitation. An aqueous solution containing metal salts is used as the electrolyte, and a negative potential is applied to induce a cathodic current through the reduction of water molecules, as represented by the equation $2\text{H}_2\text{O} + 2\text{e}^- \rightarrow \text{H}_2 + \text{OH}^-$. Utilizing the electrodeposition method, both monometallic and multimetallic LHs can be successfully prepared. For instance, NiFe-LDH nanoplates (**Figure 8**) were electrochemically deposited onto the surface of a 3D electrochemically reduced graphene oxide electrode from a mixed aqueous solution of 50 mM $\text{Ni}(\text{NO}_3)_2 \cdot 6\text{H}_2\text{O}$ and $\text{Fe}(\text{NO}_3)_3 \cdot 9\text{H}_2\text{O}$,^[85] while α -nickel hydroxide intercalated with NO_3^- was synthesized by galvanostatic cathodic reduction of an aqueous nickel nitrate solution using a nickel plate cathode.^[86] It is worth noting that the phase composition, morphology, and crystallinity of hydroxides or LDHs are significantly influenced by factors such as the type of metal salts used, temperature, deposition current, and salt concentration.^[87] One typical example is that Brownson et al.^[88] synthesized $\text{Co}(\text{OH})_2$ nanoparticles on transparent conductive oxide (TCO) substrates by localized cathodic electrogeneration of hydroxyl via the reduction of NO_2^- ion precursors in a solution containing Co^{2+} in very low concentration with a reaction time of 4000 s, and they found films deposited at 60 and 95 °C yielded $\text{Co}(\text{OH})_2$ with and without intercalated NO_3^- , respectively. Another example is that the concentration of metal salts has an important effect on the successful intercalation of anions into the structure of $\text{Ni}(\text{OH})_2$, which is reflected by the condition that $\text{Ni}(\text{OH})_2$ intercalated with and without anions can be synthesized in 0.2–1.0 M and 0.05–0.1 M NiCl_2

solution.^[89] With the above discussion in mind, it is evident that the electrodeposition method is a simple, time-efficient, and environmentally friendly approach, and has been widely regarded as one of the most effective methods for preparing LHs. However, the electrodeposition method suffers from the following disadvantages: 1, it is undoubtedly true that the electrochemical deposition technique involves the use of the substrate, leading to the formation of a thin film rather than individual nanoparticles on the substrate, which limits the application of the obtained nanomaterials in the fields that prefer individual nanoparticles; 2, the conductive solvent is one indispensable factor for the electrochemical deposition technique, and this limits the application of this technique in a non-conductive solvent (ethanol, etc.); 3, the electrochemical deposition technique is a more complicated system compared with the growth process in solution in the absence of external force, increasing the difficulty of investigating the formation mechanism via in situ techniques.

3.4. Corrosion Engineering Method

Corrosion engineering synthesis is a newly developed way for the preparation of LHs intercalated with the anions. It is similar to liquid phase synthesis except that at least one kind of metal ions was provided by pure metal or alloy instead of metallic salt. In addition to providing metal ions, the employed pure metal often serves as the hard template directing the growth of LHs intercalated with the anions. One typical example is that, as shown in **Figure 9**, Liu et al.^[90] reported that different Fe-based LDH intercalated with anions can be generated by immersing iron substrates (e.g., iron plate) in an aqueous solution containing a certain amount of divalent cations (e.g., Ni^{2+} , Co^{2+} , Mn^{2+} , or Mg^{2+}) at ambient temperature. The key to the method being successful is the introduction of suitable divalent cations in the corrosive environment, ultimately leading to the generation of nanosheet array thin films of LDH, instead of commonly-formed iron rusts, on iron substrates. The above method is usually used for the preparation of multimetallic LHs, while monometallic LHs can be obtained via the dealloying strategy of corrosion engineering synthesis. For instance, by one-step dealloying Al from an $\text{Al}_{85}\text{Co}_{14.4}\text{Pt}_{0.3}\text{Pd}_{0.3}$ precursor in NaOH solution at 0 °C, the left Co was oxidized to form ultrathin $\text{Co}(\text{OH})_2$ nanosheets. Based on the above discussion, it is easy to find that the corrosion engineering synthesis is usually carried out in an aqueous solution at around room temperature, making it energy-efficient and cost-effective. However, this route not only possesses similar disadvantages to the electrodeposition method but it cannot be applied to all LHs.

3.5. Ion Exchange Method

Synthesizing LHs intercalated with anions via the ion exchange method is completely different from other methods mentioned above because other methods involve the direct preparation of LHs while the ion exchange method entails restructuring the structure of the already formed LHs to achieve a desired outcome. Namely, the ion exchange method is generally employed as the second step to obtain new LHs which inherit the characteristics of precursors formed in the first step. For the ion exchange

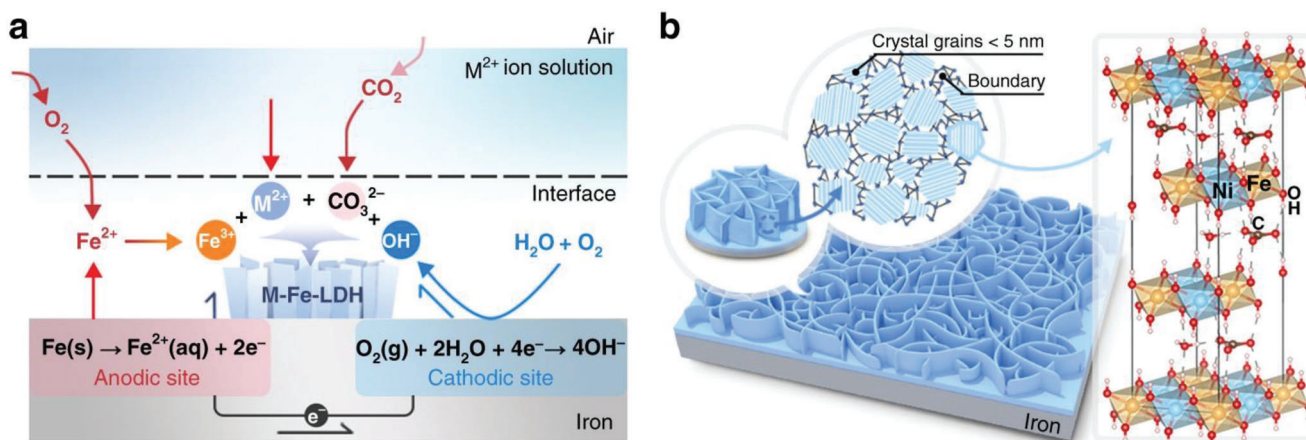


Figure 9. Schematic illustrations of the formation and microstructure of LDH via corrosion engineering synthesis. a) The specific reactions happened during the corrosion of iron substrates; b) the formation of grain boundary-enriched LDH nanosheet arrays on the surface of iron substrates. Reproduced with permission.^[90] Copyright 2018, Springer Nature.

method, the already formed LHs provide most of the factors required for the growth of new LHs, and only very few types of ions for the growth of new LHs are needed to be obtained from the reaction solution. For example, $\text{Zn}(\text{OH})_2$ intercalated with CO_3^{2-} was precipitated at $\text{pH} = 5$ from standard $3.3 \times 10^{-2} \text{ mol L}^{-1}$ ZnCl_2 and $2.4 \times 10^{-2} \text{ mol L}^{-1}$ urea solutions aged at 90°C .^[91] Considering the absence of Cl^- in the structure of $\text{Zn}(\text{OH})_2$, we infer that CO_3^{2-} competes with and prevents the intercalation of Cl^- into the structure of the final LHs, probably because of the larger charge density that improves the retention of the carbonate in the LDH.^[92] Actually, the very strong affinity of CO_3^{2-} with the $\text{M}(\text{OH})_{2-x}$ layers has been well known, which can be reflected by the fact that synthesizing LHs intercalated with non- CO_3^{2-} anions requires excluding CO_2 of air to prevent it appearing as a contamination in the final product.^[93] The above discussion indicates that different anions have different intercalation abilities in the structure of LHs. With this in mind, it is reasonable to infer that anions with weak intercalation ability can be easily replaced by other anions possessing strong intercalation ability, supported by many successful ion exchange experiments in water at room temperature. For example, the intercalation of dihydrogen phosphate or hydrogen phosphate anions into the CaFe-LDH intercalated with NO_3^- was achieved by reacting the formed LDH with an aqueous solution of KH_2PO_4 or K_2HPO_4 at room temperature under vigorous stirring.^[94] Another example is that NO_3^- of $[\text{M}_2\text{Al}(\text{OH})_6]\text{NO}_3 \cdot 2\text{H}_2\text{O}$ ($\text{M} = \text{Mg}, \text{Ca}$) can be replaced by Cl^- , CO_3^{2-} , PO_4^{3-} via simple stirring aqueous solution containing $[\text{M}_2\text{Al}(\text{OH})_6]\text{NO}_3 \cdot 2\text{H}_2\text{O}$ and sodium/ammonium salt of the suitable anion at room temperature for 5 h,^[95] indicating the weaker intercalation ability of NO_3^- than Cl^- , CO_3^{2-} and PO_4^{3-} . Although NO_3^- has a very weak affinity with the $\text{M}(\text{OH})_{2-x}$ layers compared with other anions, we can substitute NO_3^- for other anions in the structure of LHs if the reaction parameters of the ion exchange process are adjusted as needed. For instance, Liu et al. carried out the replacement of the originally intercalated Cl^- of $\alpha\text{-Co}(\text{OH})_2$ by NO_3^- and $\text{C}_{12}\text{H}_{25}\text{OSO}_3^-$ via heating an aqueous solution of $\alpha\text{-Co}(\text{OH})_2$ intercalated with Cl^- and NaNO_3 or $\text{C}_{12}\text{H}_{25}\text{OSO}_3\text{Na}$ (DS) at room temperature or 90°C under stirring and N_2 flow.^[76b] The authors found that at room

temperature, the substitution reaction for NO_3^- was incomplete even after 7 days of the reaction time, and no reaction occurred for DS anions. Interestingly, the reactions could be driven in relatively short periods at an elevated temperature, indicating the positive effect of temperature on promoting the ion exchange rate of anions with weak intercalation ability. Aside from increasing the temperature of the ion exchange process, studies have demonstrated that choosing the appropriate solvent can also optimize the intercalation ability of anions. To be specific, replacing the intercalated Cl^- in $\alpha\text{-Co}(\text{OH})_2$ by NO_3^- was successfully realized by stirring a mixture of deionized water and ethanol containing $\alpha\text{-Co}(\text{OH})_2$ intercalated with Cl^- and NaNO_3 at room temperature.^[96] Based on the above discussion, we can conclude that different anions have different intercalation abilities in the structure of LHs, and the intercalation ability for one kind of anion can be increased by tuning the reaction parameters of the ion exchange process, such as temperature and solvent. Besides, we have to acknowledge that this method can only be applied to systems that possess the appropriate precursor, thus hindering its overall applicability.

3.6. Solid Phase Synthesis

Solid phase synthesis is a method in which molecules or ions are chemically bound on a solid support material without the involvement of additional water or involving very little additional water consumption. Dry grinding via ball milling or manual grinding is one typical solid phase synthesis method, which usually involves two steps in sequence. The first step is activating the hydroxide or metallic salts or metal oxide to form a weakened crystal structure via the grinding operation, and the second step is the washing operation that can offer the required crystal water to form LDH. For example, Mafrá et al.^[97] successfully generated MgAl-LDH intercalated with NO_3^- , which involves manually grinding $\text{Mg}(\text{NO}_3)_2 \cdot 6\text{H}_2\text{O}$ and $\text{Al}(\text{NO}_3)_3 \cdot 9\text{H}_2\text{O}$ with NaOH pellets to a paste in a mortar, followed by washing the paste four times with deionized water. The as-obtained MgAl-LDH intercalated with NO_3^- was characterized in comparison with an

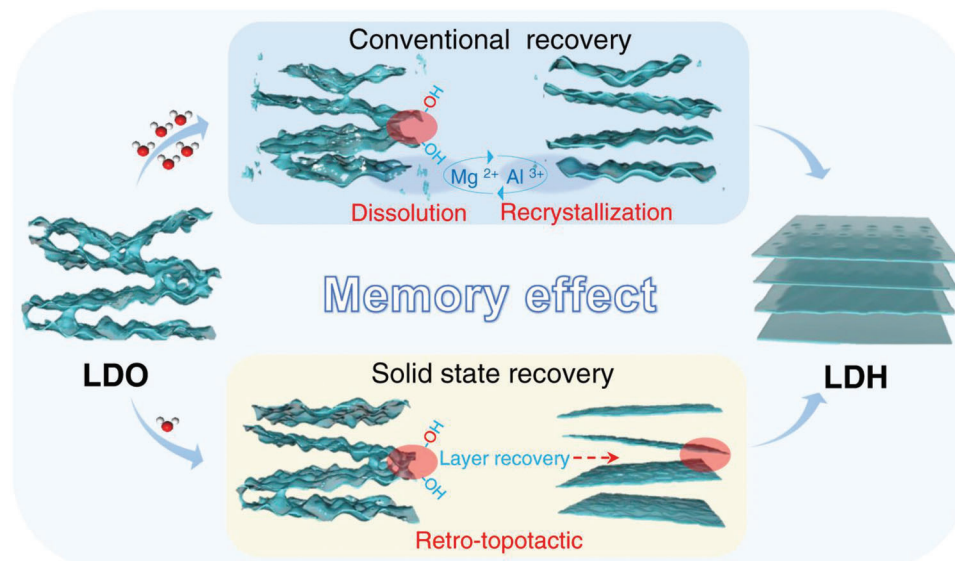


Figure 10. Schematic representation of reconstructing the structure of LDH via keeping layered double oxides (LDOs) derived from LDH. Reproduced with permission.^[98] Copyright 2022, Springer Nature.

analogous LDH prepared by the conventional co-precipitation method, and the LDH prepared via dry grinding showed all the characteristics of LDH but with a lower crystallinity, indicating that mechanochemical activation is not enough for activating the formation of a crystalline structure. Aside from mechanochemical activation, the small amount of water molecules in hydrated magnesium and aluminum nitrate salts are essential for forming such weakened crystal structures because these water molecules can provide the required monomers for structural rearrangement. It is worth noting that although the formation process described above requires washing the paste with a large amount of water, this does not necessarily mean that the formation of LDH requires a large amount of water. Actually, a small amount of water is enough for the hydroxylation of precursor, as well as interlayer water in the LDH structure, which is supported by a recent finding that layered double oxides (LDO), can restore the parent LDH structure under hydrous conditions. To be specific, Peng et al.^[98] carried out both a conventional recovery process via mixing MgAl-LDO with NaNO₃ solution in D₂O (mass ratio of MgAl-LDO to D₂O is ≈1:100) and a solid-state recovery (mass ratio of MgAl-LDO to D₂O is ≈1:1), and the structural evolution of these two processes was successfully probed by applying ex situ and in situ solid-state nuclear magnetic resonance (NMR) spectroscopy. NMR spectroscopy-derived information on local structural features indicates that recovery through aqueous solutions adheres to a dissolution-recrystallization mechanism, whereas solid-state recovery follows a retro-topotactic pathway (**Figure 10**). Compared to traditional recovery methods, solid-state recovery is faster and requires only minimal water, resulting in significantly reduced waste. As such, it may represent a more eco-friendly and cost-effective approach to producing LDH materials from LDO. Note that, during the reaction process of the above dry grinding and the solid-state recovery, the intercalation of anions into MgAl-LDH is driven by the M–OH layers' positive charge generated by partial substitution of the Mg²⁺ by Al³⁺ ions.

3.7. Other Synthetic Routes

Recently, many methods have been developed for the preparation of LDHs intercalated with anions, and some of these methods do not belong to the several routes discussed above. For instance, Duan et al.^[99] obtained LDHs intercalated with citrate, oxalate, tartrate, and malate ions free from other anions via dissolving carbonate-containing LDH precursor by the addition of the appropriate carboxylic acid followed by precipitation of the product with the help of a basic solution. Taking LDH intercalated with citrate as one example, the synthesis was performed by adding citric acid to a suspension of MgAl-LDH intercalated with carbonate dispersed in distilled water at 50 °C. The suspension slowly dissolved with effervescence and a clear solution was obtained. This solution was added dropwise to a NaOH solution maintaining a pH above 9, followed by refluxing for 2 h. This method differs significantly from ion exchange synthesis because the LDH precursor in this synthesis method is completely dissolved by acid. Actually, this method can be considered as a special liquid phase precipitation method under relatively mild conditions with the only difference being that the metal ion source comes from previously formed LDH instead of metal salts.

Another synthetic route that does not belong to the several routes discussed above is converting β-Co(OH)₂ without the intercalated anions to CoCo-LDH intercalated with Br[−] by a topochemical method.^[100] To be specific, as shown in **Figure 11**, β-Co(OH)₂ nanoplates, which were prepared via a soft-templating technique with P123 assisted, were dispersed in a solution containing Br₂ and acetonitrile, followed by magnetical shaking for one day at room temperature. The oxidative process is triggered by bromine (Br₂) and transformed the brucite-phase Co²⁺-Co²⁺ structure to a hydrotalcite-phase Co²⁺-Co³⁺ structure. At the same time, the Co–OH layers' positive charge generated by the partial substitution of the Co²⁺ by Co³⁺ ions causes the intercalation of Br[−] to maintain the electrical neutrality of CoCo-LDH. This synthesis method diverges from ion exchange synthesis because it

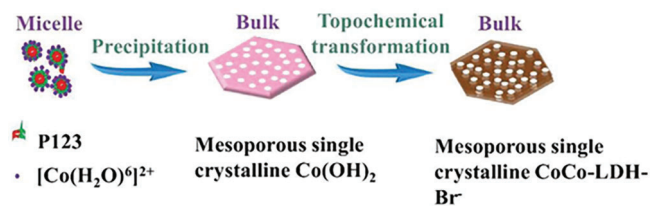


Figure 11. The schematic of the synthetic process of CoCo-LDH 2D nanomesh converted from $\text{Co}(\text{OH})_2$ nanoplates. Adapted with permission.^[100] Copyright 2019, Wiley-VCH.

involves not only a change in the oxidation state of metal ions but also the intercalation of the new guest anion, namely Br^- , without replacing the original interlayer anion. With this in mind, we can conclude that this topochemical oxidative intercalation can only be applied to the LHs containing redox-able metal elements.

It should be acknowledged that the effectiveness of this synthesis approach is limited to some systems, thereby impeding its universal application.

4. Analytical Characterization Techniques For The Intercalated Anions of LHs

As we mentioned in part 2 about the chemical composition, structure, and maintenance of electrical neutrality of LHs intercalated with guest anions, the intercalation of anions into the structure of LHs will inevitably cause a change in the interlayer spacing of LHs. Besides, the composition, size, and structure of the intercalated anions vary from one to the other. Additionally, the intercalation of anions may result in alterations to the microstructure of LHs, and the nature of these changes is contingent upon the specific type and amount of anion that is intercalated. Therefore, characterizing the intercalated anions of LHs requires identifying the above-mentioned features, which can be accomplished through the use of various analytical characterization techniques.

Powder X-ray diffraction (PXRD) is the most frequently utilized technique^[101] for characterizing the intercalated anions of LHs because it can provide the most significant and powerful evidence for confirming the existence of intercalated anions via evaluating the change of the interlayer spacing. It is well known that the interlayer spacing of LHs is equivalent to $1/(n-1)$ of the thickness along the stacking direction of the layers (n = the repetition number of the layers), which has a strong relationship with the location of a sharp basal (00X) reflection at low values of 2θ in the PXRD pattern. To be specific, the intercalation of anions into LHs results in the increase of the interlayer spacing in comparison with their counterpart without intercalated anions, which can be reflected by the diffraction peak of (00X) shifting to a lower value of 2θ . One typical example is that, as shown in **Figure 12**, the diffraction peak at 2θ values of 19° in the XRD pattern of $\beta\text{-Co}(\text{OH})_2$ without the intercalated anions is in agreement with the d -values of 4.6 Angstrom, corresponding to the distance between two adjacent stacking layers. Such a peak in the XRD pattern of $\alpha\text{-Co}(\text{OH})_2$ intercalated with anions shows a shift toward a lower angle, which indicates the increased interlayer spacing, caused by the intercalation of anions. In addition to confirming the existence of the intercalated anions, the PXRD pattern can be utilized to know the height of the gallery by subtracting the hy-

droxide layer thickness (≈ 0.48 nm) from the interlayer spacing. Considering that the gallery height depends on the size and orientation of the charge-balancing anion, the derived interlayer distance from the PXRD pattern can be regarded as evidence for recognizing the intercalated anions.^[11e] Obviously, the PXRD technique is powerful for confirming the presence and inferring the type of intercalated anions in the crystalline LHs. However, it is invalid to verify the existence of the intercalated anions in amorphous LHs due to the absence of reflection peaks in the PXRD pattern of amorphous materials with the disordered lattice.

Transmission electron microscopy (TEM) has been widely applied to characterize the morphology, crystalline structure, and elemental information of various materials.^[102] Very recently, TEM has been proven to be a powerful tool in providing information about the interlayer spacing of layered materials via observing the materials from the direction parallel to the lateral surface, then confirming the intercalation of guest anions. For example, Yuan et al. confirmed the lattice fringe spacings of metal hydroxide-organic frameworks (MHOFs) via the above-mentioned method. The obtained result (1.60 nm) is consistent with the interplanar spacings along the c axes of the structure of MHOFs computed from PXRD refinement ($c = 1.57$ nm),^[11f] supporting the validity of this method. Note that, due to the use of high voltage, confirming the interlayer spacing of LHs via TEM technique is challenging because the hydroxide is beam-sensitive, and significant structural decomposition routinely occurs under the condition of long-time electron irradiation.

Unlike TEM and XRD, which confirms the intercalation of anions by evaluating interlayer spacing, other characterization techniques provide information about the intercalated anions by investigating the composition or microstructure of the LHs. For example, infrared (IR) spectroscopy is a powerful and practical tool to obtain structural information from counter-anions located in the interlayer. To be specific, IR spectroscopy relies on the much smaller energy absorbances that occur between various vibrational and rotational states, and it is only sensitive to molecules that undergo a net change in the dipole moment during vibrational and rotational motions.^[103] Considering that most inorganic and organic anions possess a net change in the dipole moment during vibrational and rotational motions, the intercalation of guest anions can be confirmed by the presence or absence of the target anion's signal in the IR result. For instance, the existence of a carboxylic acid anion in LHs would be identified by strong antisymmetric and symmetric carboxylate stretching bands at ≈ 1560 and 1400 cm^{-1} , respectively.^[104] Alternatively, the presence of the undissociated acid in LHs would be identified by the strong absorption of the carbonyl stretch of the acid at ≈ 1700 cm^{-1} .^[105] In addition, IR allows being used to confirm the presence of carbonate or nitrate based on the presence of the peak at 1355 cm^{-1} .^[106] Note that IR is not a reliable tool for confirming the location of inorganic and organic anions, because the intercalated anions and the same type of anions adsorbed on the surface of hydroxides may present the same signal in the IR spectrum. In this case, distinguishing the intercalation or the adsorption of the target anions in the structure of LHs requires combining IR spectroscopy with other characterization techniques.

LHs without intercalated anions only consist of three elements, namely metal, oxygen, and hydrogen. By contrast, LHs with intercalated anions may contain elements other than

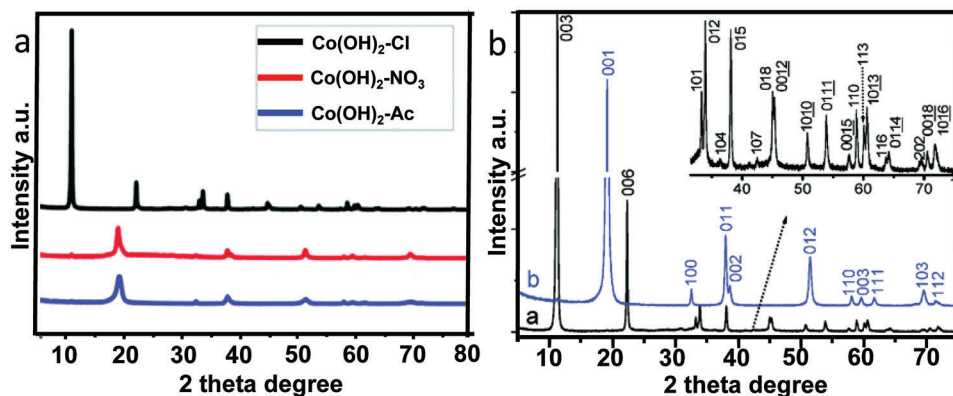


Figure 12. a) XRD patterns of α -Co(OH)₂ intercalated with Cl⁻ (black) and β -Co(OH)₂ (red Co(OH)₂-NO₃ and blue Co(OH)₂-Ac). Reproduced with permission.^[72] Copyright 2017, Royal Society of Chemistry. b) XRD patterns of α -Co(OH)₂ intercalated with Cl⁻ (black) and β -Co(OH)₂ (blue). Reproduced with permission.^[72b] Copyright 2005, American Chemical Society.

oxygen and hydrogen. Based on the element difference of LHs with and without the intercalated anions, other characterization techniques that are powerful to identify the elemental composition can be employed to verify the existence of the intercalated anions in LHs. X-ray photoelectron spectroscopy (XPS) is a surface-sensitive quantitative spectroscopy technique based on the photoelectric effect that can identify the elements that existed within a material or on its surface,^[107] has been widely used to verify the successful intercalation of inorganic or organic anions into LHs. For example, Lee et al. prepared MgAl-LDH intercalated with S containing-organic anions (L-cysteine, potassium ethyl xanthate, and sulfate sodium dodecyl) through a facile coprecipitation method at low supersaturation, and the signal of the element S displayed in the XPS survey spectrum of the obtained LDHs was regarded as one evidence for the successful intercalation of S containing-organic anions.^[108] Besides, Energy-dispersive X-ray spectroscopy (EDS or EDX), sometimes called energy-dispersive X-ray analysis (EDXA) or energy-dispersive X-ray microanalysis (EDXMA), can be used to determine the elemental composition of individual points or to map out the lateral distribution of elements from the imaged area. Especially, it has an analytical capability that can be coupled with TEM, scanning electron microscopy (SEM), and scanning transmission electron microscopy (STEM), making it possible to simultaneously observe the morphology and determine the composition. One typical example is that Bouali et al. not only characterized the morphology of the synthesized ZnAl-LDH but also confirmed the successful anion exchange of NO₃⁻ by Cl⁻ via the presence of the Cl signal in the EDS map of the product.^[109]

PXRD, TEM, IR, XPS, and EDX are routinely used characterization techniques for studying the intercalated anions of LHs, while others, such as nuclear magnetic resonance (NMR), electron paramagnetic resonance (EPR), X-ray absorption spectroscopy (XAS), ultraviolet-visible (UV-Vis) spectroscopy and quartz crystal microbalance (QCM), although reported, are less extensively employed. NMR spectroscopy is a transformational molecular characterization tool that requires little perturbation of the analyzed system while providing exceptional detail about the chemical environments of constituent atomic nuclei. The large difference in the chemical environments of elements in LHs

makes NMR a good choice for obtaining the structure information of LHs intercalated with guest anions. For example, in the first report on the study of understanding the local structure of MgAl-LDHs with the help of NMR, C. P Grey et al. employed rapid magic angle spinning (MAS) to obtain high-resolution hydrogen-1 nuclear magnetic resonance (¹H NMR) spectra and characterize the magnesium and aluminum distribution.^[110] Combining these data with ¹H-²⁷Al double-resonance and ²⁵Mg triple-quantum MAS NMR data, it is demonstrated that: 1, the cations are fully ordered for magnesium:aluminum ratios of 2:1; 2, at lower aluminum content, a nonrandom distribution of cations persists, with no Al³⁺-Al³⁺ close contacts. Besides, Yu et al. used ²H magic angle spinning (MAS) NMR spectroscopy to investigate the local structure of deuterated paramagnetic Ni²⁺-containing NiAl-LDHs for the first time.^[111] As shown in **Figure 13**, different hydrogen species, including Ni₃OD, Ni₂AlOD, and interlayer water, can be resolved in ²H NMR spectra. The authors took into account the quantitative analysis of the NMR spectra of LDHs with different Al contents and confirmed the ordering of Al³⁺ ions in the hydroxide sheets (Al-O-Al avoidance). They proposed that ²H MAS NMR spectroscopy gives new insight into different hydrogen species in paramagnetic NiAl-LDH and this approach can be extended to study the detailed structural information and properties of other paramagnetic LDHs.

Another example is Wypych et al. who prepared a zinc hydroxide nitrate (Zn₅(OH)₈(NO₃)₂·2H₂O) and a ZnAl-LDH intercalated with NO₃⁻ doped with 0.2 mol% of Cu²⁺ via a chemical precipitation method.^[112] Both compounds were intercalated with adipate (OOC(CH₂)₄COO⁻) and azelate (OOC(CH₂)₇COO⁻) ions through ion exchange reactions. The intercalation of adipate and azelate into LDH was confirmed by solid state ¹³C NMR spectroscopy, which showed only one signal of carboxylic carbon, indicating that the carboxylic ends of both acids were equivalent. However, when intercalation was performed into the matrix of Zn(OH)_{2-x} intercalated with adipate/azelate, the compound's spectrum exhibited two signals for carboxylate groups, suggesting that the intercalated adipate/azelate exists in different forms in ZnAl-LDH and Zn(OH)_{2-x} intercalated with adipate/azelate.

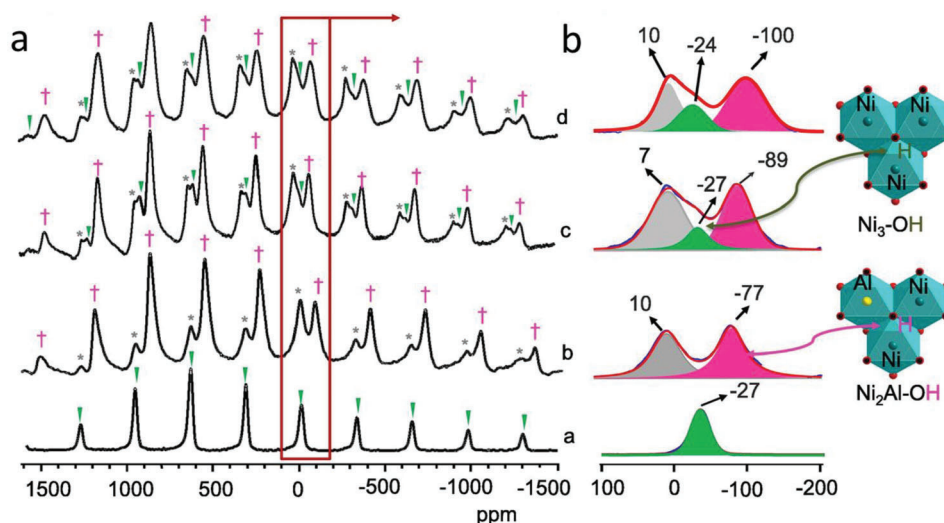


Figure 13. ^2H NMR spectra of LDHs with different molar Al contents and $\text{Ni}(\text{OH})_2$ after deuteration at a spinning speed of 20 kHz at 9.4 T showing a) the spinning sideband with manifold isotropic resonances highlighted (red box), and b) the expanded view of the isotropic resonances with simulations decomposed into each component (a: $\text{Ni}(\text{OH})_2$, b: NiAl-32.3-NO_3 , c: NiAl-25.6-NO_3 , d: NiAl-21.3-NO_3). The resonance due to water, Ni_3OD , and Ni_2AlOD are labeled in grey, green, and pink, respectively. Reproduced with permission.^[111] Copyright 2018, Elsevier.

XAS involves measuring the transmission (or fluorescence) of X-rays as a function of incrementing X-ray energy in small steps at energies close to the absorption edge. The absorption edge energy corresponds to the energy required to eject an electron from an electron shell of an element of interest. XAS is rich in information relating to local atomic states (such as oxidation states and symmetry) and neighboring atom information, including bond lengths and chemical coordination environments. As we mentioned in part 2, the intercalation of anions into LHs may result in a change in the coordination environment of metal elements in LHs, which can be easily recognized via the XAS technique. One typical example is that $\alpha\text{-Co}(\text{OH})_2$ intercalated with anions has octahedral Co^{2+} ions and additional Co^{2+} ions on tetrahedral-symmetry sites between interlayers. $\alpha\text{-Co}(\text{OH})_2$ intercalated with anions has a stronger pre-edge peak, which occurs a few elec-

tronvolts below the K-edge, compared to the $\beta\text{-Co}(\text{OH})_2$. This peak is a result of the $1 \rightarrow 3d$ absorption process, and its intensity is related to the coordination symmetry and the occupancy of the 3d shell of cobalt. To be specific, the $1 \rightarrow 3d$ transition is forbidden in an octahedral symmetry, resulting in a weak pre-edge peak, while the pre-edge peak becomes stronger in the noncentrosymmetric environment of tetrahedral cobalt.^[27] Besides, as shown in **Figure 14**, the existence of tetrahedral Co^{2+} coordination can also be verified by UV-Vis spectroscopy measurements based on the fact that the tetrahedron-containing Co compound typically exhibits peaks at lower energies because of the d-d absorption of Co^{2+} in tetrahedral coordination geometry.^[113] We have to admit that XAS and UV-Vis spectroscopy can not be applied to the investigation of all LHs, and a prerequisite for using XAS and UV-vis spectroscopy for studying such materials is the

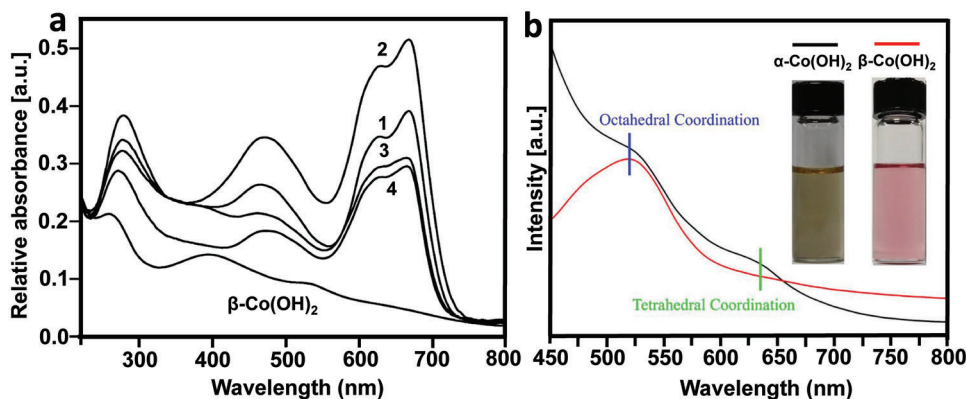


Figure 14. a) UV-visible spectra of $\alpha\text{-Co}(\text{OH})_2$ (compounds 1–4, 1: $\text{Co}_{0.80}^{\text{oct}}\text{Co}_{0.40}^{\text{tet}}(\text{OH})_2(\text{Cl})_{0.40}(\text{H}_2\text{O})_{1.1}$; 2: $\text{Co}_{0.75}^{\text{oct}}\text{Co}_{0.50}^{\text{tet}}(\text{OH})_2(\text{Cl})_{0.50}(\text{H}_2\text{O})_{0.4}$; 3: $\text{Co}_{0.84}^{\text{oct}}\text{Co}_{0.31}^{\text{tet}}(\text{OH})_2(\text{Cl})_{0.31}(\text{H}_2\text{O})_{0.3}$; 4: $\text{Co}_{0.87}^{\text{oct}}\text{Co}_{0.26}^{\text{tet}}(\text{OH})_2(\text{Cl})_{0.26}(\text{H}_2\text{O})_{1.5}$) and $\beta\text{-Co}(\text{OH})_2$ illustrating an increase in the tetrahedral Co absorbance at 640 nm as a function of Cl content. Reproduced with permission.^[75] Copyright 2009, American Chemical Society. b) UV-vis spectra of $\alpha\text{-Co}(\text{OH})_2$ and $\beta\text{-Co}(\text{OH})_2$, illustrating the presence of the signal at 640 nm for $\alpha\text{-Co}(\text{OH})_2$. Reproduced with permission.^[4c] Copyright 2014, American Chemical Society.

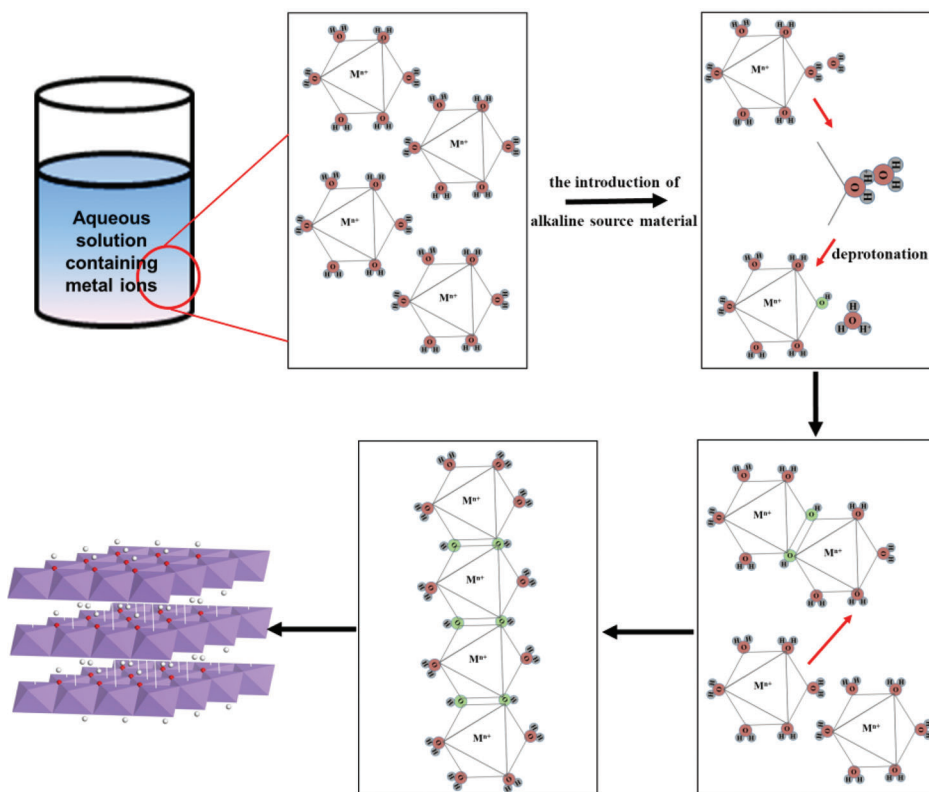


Figure 15. Illustration of the evolution process from M^{n+} ions to hydroxide in aqueous solution. Reproduced with permission.^[116] Copyright 2023, Wiley-VCH.

existence of a coordination environment difference for the target element.

The intercalation of anions into LHs involves mass variation, and some characterization techniques, such as quartz crystal microbalance (QCM), that can provide the information related to the change of mass, can also be utilized to investigate the intercalation and deintercalation behavior of guest anions. For instance, Sumio Aisawa et al.^[114] monitored dynamic intercalation behaviors of alkyl sulfate anions into MgAl-LDH by the QCM measurement, and the authors proposed that the intercalation rate was significantly influenced by alkyl chain length and concentration of the guest anions, which has led to a better understanding of the intercalation of organic anions into MgAl-LDH by ion exchange. Another example is that T. Sudare et al. first demonstrate that a 24% decrease in the filling density of ions in the interlayer space increases the nitrate storage capacity by 300%.^[115] To elucidate the mechanism underlying the high nitrate ion storage capacity, the authors carried out a comparative QCM with dissipation monitoring studies, combined with multimodal ex situ experiments and theoretical calculations, for the two LDHs with two different charge densities. It is revealed that the decreasing filling density effectively promotes the 2D hydrogen-bond networking structure in the water around interlayer nitrate ions along with a minimal change in the layered structure, resulting in a high storage capacity.

The above-mentioned ex situ techniques can provide important information related to the intercalated anions, but ex situ techniques are insufficient to understand the behavior of the

guest anions during the formation or decomposition process of LHs, especially considering the information deviation between the formation process and the finally formed structure. In this case, in situ techniques are particularly indispensable as they allow the determination of the kinetics and mechanisms of the reactions. In situ techniques are discussed in the next part together with the intercalation mechanism.

5. The Intercalation Mechanism and In Situ Techniques

Theoretically, the formation process of LHs without intercalated anions can be described as follows (see **Figure 15**): 1) Metal cations first interact with water molecules to form the hexa-aqua ions (for example, $[M(H_2O)_6]^{n+}$, M = metal cations) before adding an alkaline source. 2) As the pH rises, the hexa-aqua cations undergo a deprotonation process, condensation reactions via olation or oxolation, and elimination of water molecules, leading to the formation of an insoluble hydroxide network.^[116] As for the formation process of LHs intercalated with anions, it additionally involves both incorporating guest anions into the network of host hydroxides and accepting these guest anions by the network of host hydroxides. Therefore, understanding the intercalation mechanism strongly relies on the knowledge about the intercalation/deintercalation evolution of the target anions over time, which is usually obtained by means of analytical characterization techniques. It is well known that ex situ techniques are insufficient to understand the behavior of the guest anions

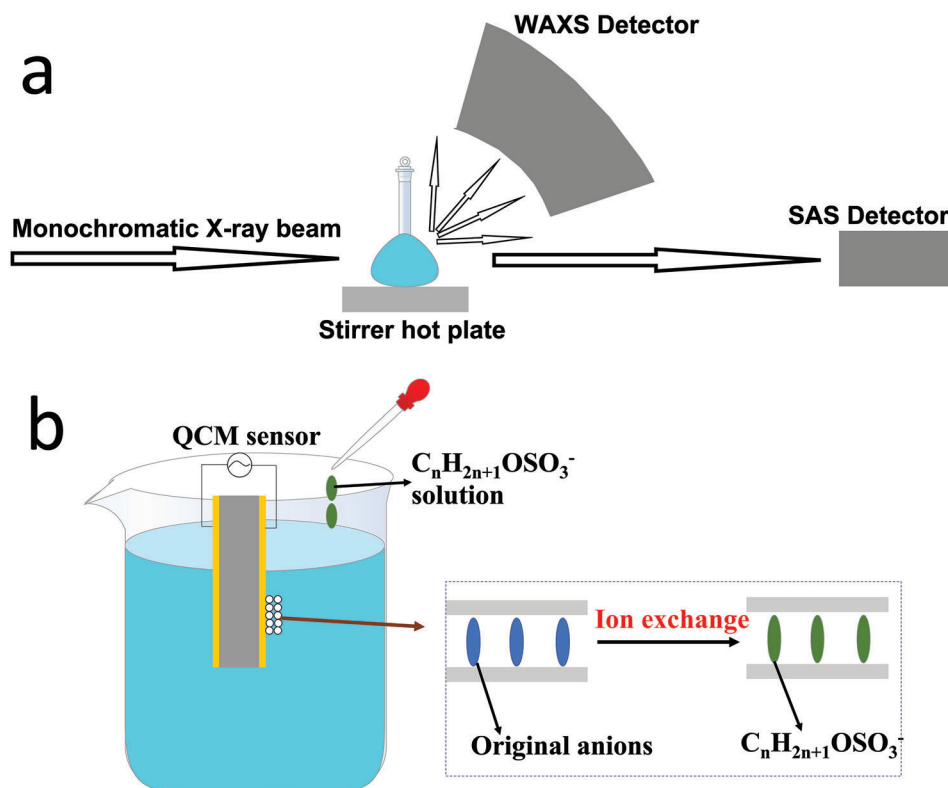


Figure 16. a) Experimental set-up used for the simultaneous time-resolved, in situ SAXS/WAXS measurement. Reproduced with permission.^[41] Copyright 2007, Royal Society of Chemistry. b) Schematic illustration of the preparation process of the LDH immobilized QC electrode and the cell for intercalation of organic sulfate anion.

during the formation process of LHs, and in situ techniques are particularly indispensable as they are important for obtaining real-time information on the kinetics and mechanism of the reactions. However, owing to the difficulty of in situ monitoring the transient intercalation process of guest anions with a small size, there are very few studies that directly investigate the intercalation process of anions during the formation process of LHs using in situ characterization techniques. For instance, so far, understanding the intercalation mechanism of guest anions into transition metal hydroxides depends on investigating the deintercalation behavior of the intercalated anions. One typical example is a kinetic study of the phase conversions of α -Co(OH)₂ intercalated with different anions, namely two pink forms (Co(OH)_{1.4}(NCO)_{0.6}·0.6H₂O, Co(OH)_{1.5}(NO₃)_{0.5}·0.6H₂O) and a green form (Co(OH)_{1.6}Cl_{0.4}·0.4H₂O), to a brucite-like β -Co(OH)₂ in the presence of NaOH was performed with the help of time-resolved in situ energy-dispersive X-ray diffraction (EDXRD) and time-resolved in situ simultaneous small/wide angle X-ray scattering (SAXS/WAXS).^[41] The used setup is shown in **Figure 16a**, and such setup allows the simultaneous observation of Bragg reflections with a wide range of *d*-spacings, which means that the proportion of starting materials, intermediate phases, and the products may be quantitatively determined throughout the course of the reaction. The kinetic data have been modeled using the Avrami-Erofe'ev model. The analysis indicates that: 1, the conversion of Co(OH)_{1.4}(NCO)_{0.6}·0.6H₂O to β -Co(OH)₂ follows a 2D diffusion-controlled model; 2, the

conversion of Co(OH)_{1.6}Cl_{0.4}·0.4H₂O to β -Co(OH)₂ is best modeled by a phase-boundary-controlled process and an Ostwald ripening model is obeyed during the final stages of the reaction; 3, the transformation from Co(OH)_{1.5}(NO₃)_{0.5}·0.6H₂O to β -Co(OH)₂ proceeds via an intermediate crystalline phase, which is thought to be an α -Co(OH)₂ with an expanded interlayer separation containing tetrahedrally coordinated Co²⁺. On the one hand, the difference in conversion mechanism for α -Co(OH)₂ intercalated with different anions implies the potential deintercalation ability difference of different anions, which is probably related to the different properties of different anions. Note that the deintercalation ability for one kind of anion is not fixed and it varies with the change of the reaction parameters, which is supported by the finding that Al-Ghoul et al. reported a kinetic study for the intercalation of Cl⁻ during the formation of α -Co(OH)₂ and its conversion to β -Co(OH)₂ within a reaction-diffusion framework (namely the diffusion of OH⁻ into a biopolymer gel containing Co from one side to the other side).^[117] The authors found that the deintercalation stops taking place when the concentration of OH⁻ is low, indicating that the deintercalation ability is tunable by changing the reaction parameters. Interestingly, the intercalation ability displays a variation trend similar to that of the deintercalation ability with changes in synthesis conditions. To be specific, as we mentioned in part 3, the study of Yin et al. revealed that different anions possess different intercalation abilities into LHs under the same synthesis condition,^[72] and the changed synthesis condition (such as tuning pH) can increase

the intercalation ability of anions.^[73] Based on the above discussion, it is reasonable to speculate that the intercalation ability of anions into LHs is strongly related to their own properties, but this intercalation ability also varies with changes in the external reaction parameters. On the other hand, in the study of the phase conversions of α -Co(OH)₂ intercalated with different anions to a brucite-like β -Co(OH)₂, keeping these α -Co(OH)₂ intercalated with different anions in NaOH solution-induced the deintercalation of anions. This inspires us to infer that the successful intercalation of anions into LHs requires not only the initial incorporation but also the final acceptance of guest anions into the host network.

Note that without involving in situ characterization techniques, there are some attempts to explore the intercalation mechanism of guest anions into Co(OH)₂. The example is that, based on ex situ characterization results for the finally formed product along with examining partial charge calculations and predicting pH-dependent stability of aqueous precursor complexes, Neilson et al. proposed that the kinetic reaction rate influences the tetrahedrally coordinated Co-associated Cl ligands occupying the sites of the hydroxide lattice.^[75] Specifically, the authors achieved kinetic control of a variable intralayer Co coordination in the layered hydroxide salt, Co^{oct}_{1-0.5x}Co^{tet}_x(OH)₂(Cl)_x(H₂O)_n (oct = octahedrally coordinated Co site, tet = tetrahedrally coordinated Co site), by using slow NH₃ diffusion across an air-water interface. They performed structural characterization on multiple-length scales in conjunction with compositional analysis, and also calculated the partial charges, and predicted the stability of the aqueous precursor complexes. The results indicated that the probability of forming Co-Cl complexes is more likely when the pH is slowly elevated while a fast reaction rate is beneficial for increasing the probability that different complexes (with or without Cl) will collide and condense via olation to form an oligomeric cluster containing different metal coordination environments. Based on the above analysis, a mechanism is proposed to reconcile the kinetic competition between the hydrolysis of soluble octahedral Co complexes and the condensation of these complexes with transiently formed tetrahedral Co complexes stabilized by the Cl ligand. Based on the above discussion, it is concluded that there is a high likelihood of anions intercalating into the structure of Co(OH)₂ at the beginning of the reaction, but this does not necessarily mean that these anions will be ultimately retained in the structure. The ability of certain anions to be retained in the structure of Co(OH)₂ is dominated by their own properties but can be drastically influenced by external factors, such as concentration, temperature, et al.

Similar to the progress of investigating the intercalation mechanism of anions into transition metal hydroxides, there have been very few studies on the intercalation mechanism of anions into LDHs by directly monitoring the intercalation process. Instead, the influence factors on the intercalation of anions are indirectly reflected by studying the guest anion exchange process. For instance, O'Hare et al.^[118] first synthesized the brucite-like Ca₂Al(OH)₆·NO₃·2H₂O using the coprecipitation method. The dicarboxylate anion 1, 4-benzenedicarboxylate was selectively intercalated into Ca₂Al(OH)₆·NO₃·2H₂O from an aqueous solution containing an equimolar mixture of the 1, 2- and 1, 4-benzenedicarboxylates. Time-resolved in situ energy-dispersive X-ray diffraction studies of the competitive intercala-

tion reaction revealed that initially both the 1, 2- and the 1, 4-benzenedicarboxylates are intercalated in the LDH, followed by replacement of the 1, 2-benzenedicarboxylate by the 1, 4-isomer as the reaction proceeds. The final thermodynamic product is Ca₂Al(OH)₆[1,4-C₈H₄O₄]_{0.5}·xH₂O.^[119] The finding of this study suggests that initially different kinds of anions may be intercalated into the interlayers of LDHs, but whether these anions can be ultimately retained is influenced by their own properties, indicating that the affinity of different anions with metal ions is different. This hypothesis is also supported by other studies. One typical example is that, as shown in Figure 16b, Sumio Aisawa et al.^[114] utilized a QCM with a MgAl-LDH thin film immobilized gold disc (LDH/QC) electrode to investigate a dynamic intercalation behavior of organic anions into the LDH interlayer by ion exchange. A stable minute LDH film was prepared by using a translucent aqueous sol of LDH containing OH⁻ ions and magnesium acetate molecules in the interlayer, which was subsequently immobilized on the gold disc after pretreatment of the surface of the supporting silica electrode with a hydrophobic agent. In the kinetic analysis, alkyl sulfates having n-alkyl chains (C_nH_{2n+1}, n = 5--12; abbreviated as C_nS) were used as guest anions. The authors found that the guest anions having a longer carbon chain can be easily intercalated into the LDH interlayer, and the intercalation rate was significantly influenced by the concentration of the guest anions. Such finding indicates that different types of anions possess different intercalation abilities at the beginning of the reaction, and their intercalation abilities can be significantly influenced by the concentration, which is consistent with the above discussion about anions intercalating into the structure of Co(OH)₂. Note that the intercalation of anions for LDHs is driven by the M-OH layers' positive charge generated by partial substitution of the M²⁺ by M³⁺ ions, which differs from the intercalation of anions for Co(OH)₂ intercalated with anion caused by the amount decrease of OH⁻ groups. Therefore, the guest anions intercalated into Co(OH)₂ may eventually deintercalate and form Co(OH)₂ without the intercalated anions, but not all guest intercalated anions in LDHs can be totally deintercalated.

6. Summary

The intercalation chemistry of LHs has great relevance for their nucleation, growth, structure, composition and size, and investigating the intercalation chemistry represents an important way to fundamental understanding and facilitating the practical application of LHs. However, researchers' attention is mainly directed to the development of the preparation and performance improvement of such materials, while less effort has been put into their fundamental understanding, such as the structure, the maintenance of electrical neutrality, the analytical characterization techniques, and the intercalation mechanism. Considering the importance of "insight must precede application" and the guidance effect of one in-depth review for scientists in the area, we present a systematic introduction of the recent progress of the fundamental understanding of LHs intercalated with guest anions. To be specific, we introduced the chemical composition, structure, and maintenance of electrical neutrality of transition metal hydroxides intercalated with anions and LDHs. Furthermore, considering the rapid development in the field of preparing LHs

intercalated with guest anions, we provided a timely summary of the recent progress in their preparation via the bottom-up approach and discussed not only the potential impact of external reaction parameters on the intercalation or non-intercalation of anions into LHs but also the advantages and disadvantages of each synthesis method. We also discussed the analytical characterization techniques for LHs intercalated with guest anions, including PXRD, TEM, IR, XPS, EDX, XAS, UV-Vis, QCM, etc. Besides, although progress is slow in exploring the intercalation mechanism and the number of studies in this field is small, we included as many examples as possible in this review and inferred the possible intercalation mechanism.

Although significant progress has been made in the field of LHs intercalated with guest anions, there are still numerous challenges to be addressed for the further development and effective utilization of such materials. First, the existing synthesis strategies vary from one system to the other, prohibiting a universal preparation, and new synthesis strategies are required to overcome this challenge. Second, several technical drawbacks associated with current synthesis methods, including high costs, tedious operation, non-green solvents, and possible contamination, limit their widespread application, which motivates us to improve the synthesis scheme. Third, the application performance of LHs intercalated with guest anions is determined by the amount of intercalated anions, emphasizing the need to optimize synthesis routes to achieve controlling the intercalated amount of guest anions. Solving the above-mentioned problems requires a complete and thorough understanding of the intercalation mechanism, which depends on the emergence of appropriate in situ characterization methods for observing the intercalation process. So far, there is a lack of appropriate in situ characterization methods to study the intercalation mechanism of anions, especially no experimental techniques that can directly monitor the intercalation and deintercalation processes of anions. Nonetheless, by using a combination of characterization methods, it is possible to create a fairly comprehensive depiction of the intricate mechanisms involved in the intercalation/deintercalation process of guest anions.

The scientific community has yet to fully explore this remarkable group of materials, which offers intriguing multifunctional properties and a broad range of potential applications. We hope this review can not only act as a platform that can help researchers to easily and quickly learn about the development in fundamental understanding and materials preparation of LHs intercalated with guest anions but also draw more attention to identify and then solve the existing problems in this field.

Acknowledgements

This research was funded by the Sino-German Center for Research Promotion and the Deutsche Forschungsgemeinschaft DFG (Grants GZ 1351 and CO194/19-1).

Open access funding enabled and organized by Projekt DEAL.

Conflict of Interest

The authors declare no conflict of interest.

Author Contributions

The manuscript was written through the contributions of all authors. All authors have approved the final version of the manuscript.

Keywords

intercalated anions, intercalation chemistry, layered hydroxides, structures

Received: January 17, 2023

Revised: May 6, 2023

Published online: June 4, 2023

- [1] a) Z. Yan, H. Sun, X. Chen, H. Liu, Y. Zhao, H. Li, W. Xie, F. Cheng, J. Chen, *Nat. Commun.* **2018**, *9*, 2373; b) R. Z. Ma, T. Sasaki, *Acc. Chem. Res.* **2015**, *48*, 136; c) H. Yin, Z. Tang, *Chem. Soc. Rev.* **2016**, *45*, 4873; d) Z. Hu, X. Xiao, H. Jin, T. Li, M. Chen, Z. Liang, Z. Guo, J. Li, J. Wan, L. Huang, Y. Zhang, G. Feng, J. Zhou, *Nat. Commun.* **2017**, *8*, 15630; e) J. R. Ran, J. Zhang, J. G. Yu, M. Jaroniec, S. Z. Qiao, *Chem. Soc. Rev.* **2014**, *43*, 7787; f) D. Wang, D. Astruc, *Chem. Soc. Rev.* **2017**, *46*, 816; g) B. Su, Z. C. Cao, Z. J. Shi, *Acc. Chem. Res.* **2015**, *48*, 886; h) H. F. Wang, C. Tang, B. Wang, B. Q. Li, Q. Zhang, *Adv. Mater.* **2017**, *29*, 1702327; i) S. A. Patil, D. V. Shinde, I. Lim, K. Cho, S. S. Bhande, R. S. Mane, N. K. Shrestha, J. K. Lee, T. H. Yoon, S. H. Han, *J. Mater. Chem. A* **2015**, *3*, 7900.
- [2] a) X. Long, Z. Wang, S. Xiao, Y. An, S. Yang, *Mater. Today* **2016**, *19*, 213; b) G. Chen, H. Wan, W. Ma, N. Zhang, Y. Cao, X. Liu, J. Wang, R. Ma, *Adv. Energy Mater.* **2020**, *10*, 1902535; c) H. T. Tan, W. Sun, L. Wang, Q. Yan, *ChemNanoMat* **2016**, *2*, 562; d) J. E. ten Elshof, H. Yuan, P. Gonzalez Rodriguez, *Adv. Energy Mater.* **2016**, *6*, 1600355; e) T. Nguyen, M. d. F. Montemor, *Adv. Sci.* **2019**, *6*, 1801797; f) Z. Chen, R. Schmid, X. Wang, M. Fu, Z. Han, Q. Fan, E. Scheer, M. Huang, P. Nielaba, H. Cölfen, *Nat Synth* **2023**, <https://doi.org/10.1038/s44160-023-00281-y>; g) Z. Chen, X. Wang, Z. Han, S. Zhang, S. Pollastri, Q. Fan, Z. Qu, D. Sarker, C. Scheu, M. Huang, H. Cölfen, *Angew. Chem., Int. Ed.* **2023**, *62*, 2022157; h) Z. Chen, M. Huang, H. Cölfen, *CrystEngComm* **2021**, *23*, 3794.
- [3] a) J. A. Carrasco, R. Sanchis-Gual, A. S. D. Silva, G. Abellán, E. Coronado, *Chem. Mater.* **2019**, *31*, 6798; b) L. Yang, Z. Liu, S. Zhu, L. Feng, W. Xing, *Mater. Today Phys.* **2021**, *16*, 100292; c) Y. K. Kim, W. T. Jun, D. H. Youn, J. S. Lee, *J. Alloys Compd.* **2022**, *901*, 163689; d) Z. Chen, X. Wang, S. Keßler, Q. Fan, M. Huang, H. Cölfen, *J Energy Chem* **2022**, *71*, 89.
- [4] a) C. Yan, Z. Fang, C. Lv, X. Zhou, G. Chen, G. Yu, *ACS Nano* **2018**, *12*, 8670; b) Y. Zhang, J. Cao, J. Li, Z. Yuan, D. Li, L. Wang, W. Han, *Chem. Eng. J.* **2022**, *430*, 132992; c) L. Wang, C. Lin, F. Zhang, J. Jin, *ACS Nano* **2014**, *8*, 3724.
- [5] a) Y. Yu, J. Shi, X. Zhao, Z. Yuan, C. Lu, J. Lu, *Analyst* **2016**, *141*, 3305; b) J. Yu, Q. Wang, D. O'Hare, L. Sun, *Chem. Soc. Rev.* **2017**, *46*, 5950; c) Y. Liu, W. Sun, J. Xiao, Y. Fu, B. Shi, C. Lü, *Appl. Clay Sci.* **2022**, *229*, 106662.
- [6] a) Z. Matusinovic, C. A. Wilkie, *J. Mater. Chem.* **2012**, *22*, 18701; b) L. L. Zhou, W. X. Li, H. B. Zhao, J. S. Wang, B. Zhao, *Polym. Degrad. Stab.* **2022**, *204*, 110104.
- [7] L. Yu, J. F. Yang, B. Y. Guan, Y. Lu, X. W. Lou, *Angew. Chem., Int. Ed.* **2018**, *57*, 172.
- [8] D. J. Lee, S.-H. Yu, H. S. Lee, A. Jin, J. Lee, J. E. Lee, Y.-E. Sung, T. Hyeon, *J. Mater. Chem. A* **2017**, *5*, 8744.
- [9] X. Zou, Y. Liu, G. D. Li, Y. Wu, D. P. Liu, W. Li, H. W. Li, D. Wang, Y. Zhang, X. Zou, *Adv. Mater.* **2017**, *29*, 1700404.
- [10] Y. Zhao, X. Zhang, X. Jia, G. I. Waterhouse, R. Shi, X. Zhang, F. Zhan, Y. Tao, L. Z. Wu, C. H. Tung, *Adv. Energy Mater.* **2018**, *8*, 1703585.

- [11] a) X. Kang, H. Ye, *Cem. Concr. Compos.* **2022**, *130*, 104533; b) M. Szabados, A. Gácsi, Y. Gulyás, Z. Kónya, Á. Kukovecz, E. Csányi, I. Pálinkó, P. Sipos, *Appl. Clay Sci.* **2021**, *212*, 106233; c) A. N. Narayanappa, S. Nagendran, P. V. Kamath, *New J. Chem.* **2021**, *45*, 5837; d) J. Ma, J. Xia, Z. Liang, X. Chen, Y. Du, C. H. Yan, *Small* **2021**, *17*, 2104423. e) B. M. Hunter, W. Hieringer, J. Winkler, H. Gray, A. Müller, *Energy Environ. Sci.* **2016**, *9*, 862; f) S. Yuan, J. Peng, B. Cai, Z. Huang, A. T. Garcia-Esparza, D. Sokaras, Y. Zhang, L. Giordano, K. Akkiraju, Y. G. Zhu, *Nat. Mater.* **2022**, *21*, 673; g) T. Hu, Z. Gu, G. R. Williams, M. Strimaite, J. Zha, Z. Zhou, X. Zhang, C. Tan, R. Liang, *Chem. Soc. Rev.* **2022**, *51*, 6126; h) D. P. Sahoo, K. K. Das, S. Mansingh, S. Sultana, K. Parida, *Coord. Chem. Rev.* **2022**, *469*, 214666; i) Y. Cao, D. Zheng, F. Zhang, J. Pan, C. Lin, *J. Mater. Sci. Technol.* **2022**, *102*, 232; j) S. Omwoma, W. Chen, R. Tsunashima, Y. F. Song, *Coord. Chem. Rev.* **2014**, *258*, 58; k) X. Lu, H. Xue, H. Gong, M. Bai, D. Tang, R. Ma, T. Sasaki, *Nano-Micro Lett.* **2020**, *12*, 1.
- [12] S. Nakagaki, G. S. Machado, J. F. Stival, E. H. dos Santos, G. M. Silva, F. Wypych, *Prog. Solid State Chem.* **2021**, *64*, 100335.
- [13] L. Desgranges, G. Calvarin, G. Chevrier, *Acta Crystallogr. B. Struct. Sci.* **1996**, *52*, 82.
- [14] W. R. Busing, H. A. Levy, *J. Chem. Phys.* **1957**, *26*, 563.
- [15] Q. Zhao, H. J. Kulik, *J. Chem. Theory Comput.* **2018**, *14*, 670.
- [16] R. Wyckoff, *Crystal structures* **1963**, *1*, 85.
- [17] W. Lotmar, W. Feitknecht, *Z Kristallogr Cryst Mater* **1936**, *93*, 368.
- [18] R. Cairns, E. Ott, *J. Am. Chem. Soc.* **1933**, *55*, 527.
- [19] M. Baneeva, S. Popova, *Geokhimiya* **1969**, *1969*, 1014.
- [20] Cd(OH)₂, <https://www.materialsproject.org/materials/mp-625548> (accessed: October 2022).
- [21] Cu(OH)₂, <https://www.materialsproject.org/materials/mp0505105/> (accessed: October 2022).
- [22] a) H. Yan, X. J. Zhao, Y. Q. Zhu, M. Wei, D. G. Evans, X. Duan, The periodic table II: catalytic, materials, biological and medical applications **2019**, 89; b) Metal hydroxide, https://www.en.wikipedia.org/wiki/Metal_hydroxide (accessed: June 2022).
- [23] What Exactly do I have – Dolomite, Limestone or Dolostone?, <https://www.georarity.com/blog/> (accessed: January 2023).
- [24] G. G. C. Arizaga, K. G. Satyanarayana, F. Wypych, *Solid State Ion* **2007**, *178*, 1143.
- [25] Mg₂(OH)₃NO₃ (Mg₂[NO₃][OH]₃ hex) Crystal Structure, https://www.materials.springer.com/isp/crystallographic/docs/sd_1910454 (accessed: October 2016).
- [26] Co₂(OH)₃NO₃ (Co₂[NO₃][OH]₃) Crystal Structure, https://www.materials.springer.com/isp/crystallographic/docs/sd_1719889 (accessed: October 2016).
- [27] R. Ma, Z. Liu, K. Takada, K. Fukuda, Y. Ebina, Y. Bando, T. Sasaki, *Inorg. Chem.* **2006**, *45*, 3964.
- [28] Ni₂(OH)₃NO₃ (Ni₂[NO₃][OH]₃) Crystal Structure, https://www.materials.springer.com/isp/crystallographic/docs/sd_1102603 (accessed: October 2016).
- [29] F. C. Hawthorne, E. Sokolova, *Can. Mineral.* **2002**, *40*, 939.
- [30] W. Stählin, H. R. Oswald, *Acta Crystallogr B Struct Sci Cryst Eng Mater* **1970**, *26*, 860.
- [31] L. A. Groat, *Am. Mineral.* **1996**, *81*, 238.
- [32] Zn₅(OH)₈(NO₃)₂ (Zn₅[NO₃]₂[OH]₈) Crystal Structure, https://www.materials.springer.com/isp/crystallographic/docs/sd_1501778 (accessed: October 2016).
- [33] Zn₃(OH)₄(NO₃)₂ (Zn₃[NO₃]₂[OH]₄) Crystal Structure, https://www.materials.springer.com/isp/crystallographic/docs/sd_1910453 (accessed: October 2016).
- [34] H. Effenberger, *Z Kristallogr Cryst Mater* **1983**, *165*, 127.
- [35] F. Hawthorne, L. Groat, *Am. Mineral.* **1985**, *70*, 1050.
- [36] H. Effenberger, *Neues Jahrbuch für Mineralogie Monatshefte* **1986**, *101*.
- [37] a) H. Oswald, *Z Kristallogr Cryst Mater* **1961**, *116*, 210; b) B. Bovio, S. Locchi, *J. Crystallogr. Spectrosc. Res.* **1982**, *12*, 507; c) J. Minceva-Stefanova, I. Kostov, *C R Acad Bulg Sci* **2002**, *55*, 57.
- [38] R. E. Bevins, S. Turgoose, P. A. Williams, *Mineral. Mag.* **1982**, *46*, 51.
- [39] R. Rojas, D. Kovacheva, K. Petrov, *Chem. Mater.* **1999**, *11*, 3263.
- [40] M. Meyn, K. Beneke, G. Lagaly, *Inorg. Chem.* **1993**, *32*, 1209.
- [41] Y. Du, K. M. Ok, D. O'Hare, *J. Mater. Chem.* **2008**, *18*, 4450.
- [42] a) W. Ostwald, *Z Phys Chem* **1897**, *22*, 289; b) W. T. Reichle, *Solid State Ion.* **1986**, *22*, 135.
- [43] ZMg₄Al₂(OH)₁₂Cl₂(H₂O)₂ (Mg₂AlCl[OH]₆[H₂O]) Crystal Structure, https://www.materials.springer.com/isp/crystallographic/docs/sd_1248474 (accessed: October 2016).
- [44] ZMg₆Fe₂(OH)₁₆CO₃·4H₂O (Mg_{0.75}Fe_{0.25}[CO₃]_{0.125}[OH]₂[H₂O]_{0.5} 2H) Crystal Structure, https://www.materials.springer.com/isp/crystallographic/docs/sd_1903897 (accessed: October 2016).
- [45] ZZn₄Al₂(OH)₁₂(CO₃)·3H₂O (Zn_{0.67}Al_{0.33}[CO₃]_{0.167}[OH]₂[H₂O]_{0.5} hex) Crystal Structure, https://www.materials.springer.com/isp/crystallographic/docs/sd_1811726 (accessed: October 2016).
- [46] Z[Zn-Al-NO₃]_{0.33} LDH (Zn_{0.67}Al_{0.33}[NO₃]_{0.33}[OH]₂[H₂O]_{0.85}) Crystal Structure, https://www.materials.springer.com/isp/crystallographic/docs/sd_1640075 (accessed: October 2016).
- [47] ZMg₆Cr₂CO₃(OH)₁₆·4H₂O (Mg_{0.75}Cr_{0.25}[CO₃]_{0.125}[OH]₂[H₂O]_{0.5} rhom) Crystal Structure, https://www.materials.springer.com/isp/crystallographic/docs/sd_1226061 (accessed: October 2016).
- [48] ZNi₄Al₂(OH)₁₂CO₃·3H₂O (Ni_{0.67}Al_{0.33}[CO₃]_{0.17}[OH]₂[H₂O]_{0.5}) Crystal Structure, https://www.materials.springer.com/isp/crystallographic/docs/sd_1622708 (accessed: October 2016).
- [49] ZH₂O₂(H₂O)_{0.61}(CO₃)_{0.16}Ni_{0.70}Fe_{0.30}O₂ (H₂O₂Fe_{0.30}Ni_{0.70}[CO₃]_{0.16}O₂[H₂O]_{0.61}) Crystal Structure, https://www.materials.springer.com/isp/crystallographic/docs/sd_1503060 (accessed: October 2016).
- [50] A. E. Stamate, O. D. Pavel, R. Zavoianu, I. C. Marcu, *Catalysts* **2020**, *10*, 57.
- [51] a) F. Fathabadi, F. Manteghi, *Chem. Proc* **2021**, *3*, x; b) T. Sudare, S. Tamura, M. Kashiwazaki, Y. Nakamura, K. Kawaguchi, H. Shiiba, K. Fujisawa, M. Tiplpook, H. Tanaka, F. Hayashi, *Adv. Mater. Interfaces* **2022**, *9*, 2201484.
- [52] S. J. Palmer, R. L. Frost, T. Nguyen, *Coord. Chem. Rev.* **2009**, *253*, 250.
- [53] a) F. P. de Sá, B. N. Cunha, L. M. Nunes, *Chem. Eng. J.* **2013**, *215*, 122; b) F. M. Vichi, O. L. Alves, *J. Mater. Chem.* **1997**, *7*, 1631.
- [54] G. Alberti, J. L. Atwood, *Solid-state supramolecular chemistry: two- and three-dimensional inorganic networks*, Pergamon Press, Oxford, UK **1996**.
- [55] E. L. Crepaldi, P. C. Pavan, J. B. Valim, *J. Braz. Chem. Soc.* **2000**, *11*, 64.
- [56] L. Pesic, S. Salipurovic, V. Markovic, D. Vucelic, W. Kagunya, W. Jones, *J. Mater. Chem.* **1992**, *2*, 1069.
- [57] a) C. Qiao, Y. Zhang, Y. Zhu, C. Cao, X. Bao, J. Xu, *J. Mater. Chem. A* **2015**, *3*, 6878; b) X. Xiong, Y. Zhao, R. Shi, W. Yin, Y. Zhao, G. I. Waterhouse, T. Zhang, *Sci. Bull.* **2020**, *65*, 987.
- [58] a) L. Qian, Z. Lu, T. Xu, X. Wu, Y. Tian, Y. Li, Z. Huo, X. Sun, X. Duan, *Adv. Energy Mater.* **2015**, *5*, 1500245; b) J. M. Gonçalves, P. R. Martins, L. Angnes, K. Araki, *New J. Chem.* **2020**, *44*, 9981.
- [59] a) H. N. Tran, C. C. Lin, H.-P. Chao, *Sep. Purif. Technol.* **2018**, *192*, 36; b) H. N. Tran, C.-C. Lin, S. H. Woo, H. P. Chao, *Appl. Clay Sci.* **2018**, *154*, 17; c) T. Kameda, S. Saito, Y. Umetsu, *Sep. Purif. Technol.* **2005**, *47*, 20; d) A. Clearfield, M. Kieke, J. Kwan, J. Colon, R. C. Wang, *J Incl Phenom Macrocycl Chem* **1991**, *11*, 361; e) N. Iyi, K. Tamura, H. Yamada, *J. Colloid Interface Sci.* **2009**, *340*, 67; f) T. Kameda, T. Yamazaki, T. Yoshioka, *Microporous Mesoporous Mater.* **2008**, *114*, 410; g) M. Bouraada, M. S. Ouali, L. C. de Menorval, *J. Saudi Chem. Soc.* **2016**, *20*, 397; h) J. M. Oh, S. Y. Kwak, J. H. Choy, *J. Phys. Chem. Solids* **2006**, *67*, 1028; i) S. Samuei, F. A. Rad, Z. Rezvani, *Appl. Clay*

- Sci.* **2020**, 184, 105388; j) W. Ding, G. Gu, W. Zhong, W. C. Zang, Y. Du, *Chem. Phys. Lett.* **1996**, 262, 259.
- [60] L. Bindi, A. G. Christy, S. J. Mills, M. E. Ciriotti, E. Bittarello, *Can. Mineral.* **2015**, 53, 791.
- [61] S. Mills, A. Christy, J.-M. Génin, T. Kameda, F. Colombo, *Mineral. Mag.* **2012**, 76, 1289.
- [62] a) Z. Chen, Q. Fan, M. Huang, H. Cölfen, *CrystEngComm* **2022**, 24, 4639; b) H. Yi, S. Liu, C. Lai, G. Zeng, M. Li, X. Liu, B. Li, X. Huo, L. Qin, L. Li, *Adv. Energy Mat.* **2021**, 11, 2002863.
- [63] a) R. Bhusari, J.-S. Thomann, J. Guillot, R. Leturcq, *J. Cryst. Growth* **2021**, 570, 126225; b) M. Bukhtiyarova, *J. Solid State Chem.* **2019**, 269, 494.
- [64] N. Kozai, H. Mitamura, H. Fukuyama, F. Esaka, S. Komarneni, *Microporous Mesoporous Mater.* **2006**, 89, 123.
- [65] S. Möhmel, I. Kurzwski, D. Uecker, D. Müller, W. Gessner, *Cryst. Res. Technol.: J. Experim. Industr. Crystallogr.* **2002**, 37, 359.
- [66] M. Gao, W. Sheng, Z. Zhuang, Q. Fang, S. Gu, J. Jiang, Y. Yan, *J. Am. Chem. Soc.* **2014**, 136, 7077.
- [67] H. Chen, J. Jiang, L. Zhang, Y. Zhao, D. Guo, Y. Ruan, D. Xia, *ChemPlusChem* **2015**, 80, 181.
- [68] G.-X. Tong, F.-T. Liu, W.-H. Wu, J.-P. Shen, X. Hu, Y. Liang, *CrystEngComm* **2012**, 14, 5963.
- [69] Y. Ding, H. Zhao, Y. Sun, G. Zhang, H. Wu, Y. Qian, *Int. J. Inorg. Mater.* **2001**, 2, 151.
- [70] J. Li, Z. Li, F. Zhan, M. Shao, *Chem. Sci.* **2021**, 12, 1756.
- [71] K. Zhu, H. Liu, M. Li, X. Li, J. Wang, X. Zhu, W. Yang, *J. Mater. Chem. A* **2017**, 5, 7753.
- [72] F. Lyu, Y. Bai, Q. Wang, L. Wang, X. Zhang, Y. Yin, *Dalton Trans.* **2017**, 46, 10545.
- [73] Z. A. Hu, Y. L. Xie, Y. X. Wang, L. J. Xie, G. R. Fu, X. Q. Jin, Z. Y. Zhang, Y. Y. Yang, H. Y. Wu, *J. Phys. Chem. C* **2009**, 113, 12502.
- [74] C. Faure, C. Delmas, M. Fouassier, *J. Power Sources* **1991**, 35, 279.
- [75] J. R. Neilson, B. Schwenzer, R. Seshadri, D. E. Morse, *Inorg. Chem.* **2009**, 48, 11017.
- [76] a) H. Wang, J. Gao, Z. Li, Y. Ge, K. Kan, K. Shi, *CrystEngComm* **2012**, 14, 6843; b) Z. Liu, R. Ma, M. Osada, K. Takada, T. Sasaki, *J. Am. Chem. Soc.* **2005**, 127, 13869.
- [77] H. Huang, J. Lai, J. Lu, Z. Li, *AIP Adv.* **2019**, 9, 015307.
- [78] T. Gera, E. Nagy, T. Smausz, J. Budai, T. Ajtai, F. Kun-Szabó, Z. Homik, J. Kopniczky, Z. Bozóki, P. Szabó-Révész, *Sci. Rep.* **2020**, 10, 15806.
- [79] C. Liang, T. Sasaki, Y. Shimizu, N. Koshizaki, *Chem. Phys. Lett.* **2004**, 389, 58.
- [80] C. Liang, Y. Shimizu, M. Masuda, T. Sasaki, N. Koshizaki, *Chem. Mater.* **2004**, 16, 963.
- [81] S. Komarneni, Q. Li, R. Roy, *J. Mater. Res.* **1996**, 11, 1866.
- [82] J. Rivera, G. Fetter, P. Bosch, *Microporous Mesoporous Mater.* **2006**, 89, 306.
- [83] L. Lv, Z. Yang, K. Chen, C. Wang, Y. Xiong, *Adv. Energy Mater.* **2019**, 9, 1803358.
- [84] W. Yang, Y. Feng, N. Wang, H. Yuan, D. Xiao, *J. Alloys Compd.* **2015**, 644, 836.
- [85] X. Yu, M. Zhang, W. Yuan, G. Shi, *J. Mater. Chem. A* **2015**, 3, 6921.
- [86] R. Jayashree, P. Vishnu Kamath, *J. Appl. Electrochem.* **2001**, 31, 1315.
- [87] a) J. Tizfahm, B. Safibonab, M. Aghazadeh, A. Majdabadi, B. Sabour, S. Dalvand, *Colloids Surf A Physicochem Eng Asp* **2014**, 443, 544; b) Y. Wang, D. Cao, G. Wang, S. Wang, J. Wen, J. Yin, *Electrochim. Acta* **2011**, 56, 8285; c) I. Gualandi, M. Monti, E. Scavetta, D. Tonelli, V. Prevot, C. Mousty, *Electrochim. Acta* **2015**, 152, 75.
- [88] J. R. Brownson, C. Lévy-Clément, *Electrochim. Acta* **2009**, 54, 6637.
- [89] J. Zhang, S. Feng, *Int. J. Hydrog. Energy* **2021**, 46, 41.
- [90] Y. Liu, X. Liang, L. Gu, Y. Zhang, G.-D. Li, X. Zou, J.-S. Chen, *Nat. Commun.* **2018**, 9, 2609.
- [91] F. Sigoli, M. R. Davolos, M. Jafelicci Jr, *J. Alloys Compd.* **1997**, 262, 292.
- [92] S. Carlino, *Solid State Ion* **1997**, 98, 73.
- [93] H. Yan, J. Wang, Y. Zhang, W. Hu, *J. Alloys Compd.* **2016**, 678, 171.
- [94] M. A. Woo, T. W. Kim, M.-J. Paek, H.-W. Ha, J.-H. Choy, S.-J. Hwang, *J. Solid State Chem.* **2011**, 184, 171.
- [95] A. Radha, P. V. Kamath, C. Shivakumara, *Solid State Sci.* **2005**, 7, 1180.
- [96] J. Cheng, L. Liu, J. Zhang, F. Liu, X. Zhang, *J. Electroanal. Chem.* **2014**, 722, 23.
- [97] A. N. Ay, B. Zümreoglu-Karan, L. Mafra, *Z. Anorg. Allg. Chem.* **2009**, 635, 1470.
- [98] L. Jin, X. Zhou, F. Wang, X. Ning, Y. Wen, B. Song, C. Yang, D. Wu, X. Ke, L. Peng, *Nat. Commun.* **2022**, 13, 6093.
- [99] J. Zhang, F. Zhang, L. Ren, D. G. Evans, X. Duan, *Mater. Chem. Phys.* **2004**, 85, 207.
- [100] M. Qin, S. Li, Y. Zhao, C. Y. Lao, Z. Zhang, L. Liu, F. Fang, H. Wu, B. Jia, Z. Liu, *Adv. Energy Mat.* **2019**, 9, 1803060.
- [101] a) P. Kowalik, M. Konkol, M. Kondracka, W. Próchniak, R. Bicki, P. Wiercioch, *Appl. Catal. A Gen* **2013**, 464, 339; b) Z. Wang, W. Liu, Y. Hu, L. Xu, M. Guan, J. Qiu, Y. Huang, J. Bao, H. Li, *Inorg. Chem. Front.* **2019**, 6, 1890.
- [102] a) M. Schorb, I. Haberbosch, W. J. Hagen, Y. Schwab, D. N. Mastronarde, *Nat. Methods* **2019**, 16, 471; b) A. Rizvi, J. T. Mulvey, B. P. Carpenter, R. Talosig, J. P. Patterson, *Chem. Rev.* **2021**, 121, 14232; c) F. Hage, G. Radtke, D. Kepaptsoglou, M. Lazzeri, Q. Ramasse, *Science* **2020**, 367, 1124; d) B. Han, Y. Zou, Z. Zhang, X. Yang, X. Shi, H. Meng, H. Wang, K. Xu, Y. Deng, M. Gu, *Nat. Commun.* **2021**, 12, 3066; e) J. T. van Omme, H. Wu, H. Sun, A. F. Beker, M. Lemang, R. G. Spruit, S. P. Maddala, A. Rakowski, H. Friedrich, J. P. Patterson, *J. Mater. Chem. C* **2020**, 8, 10781.
- [103] P. Loubeyre, F. Occelli, P. Dumas, *Nature* **2020**, 577, 631.
- [104] H. Nabipour, Y. Hu, *J. Porous Mater.* **2022**, 29, 341.
- [105] T. Kondratenko, O. Ovchinnikov, I. Grevtseva, M. Smirnov, O. Erina, V. Khokhlov, B. Darinsky, E. Tatianina, *Materials* **2020**, 13, 909.
- [106] Y. Cao, S. Fang, K. Chen, H. Qi, X. Zhang, C. Huang, J. Wang, J. Liu, *Appl. Sci.* **2022**, 12, 4492.
- [107] T. Soe, A. Jityen, T. Kongkaew, K. Subannajui, A. Sinsarp, T. Osotchan, *AIP Conf. Proc.* **2020**, 2279, 140002.
- [108] S. T. Lin, H. N. Tran, H. P. Chao, J. F. Lee, *Appl. Clay Sci.* **2018**, 162, 443.
- [109] A. C. Bouali, M. H. Iuzviuk, M. Serdechnova, K. A. Yasakau, D. F. Wieland, G. Dovzhenko, H. Maltanova, I. A. Zobkalo, M. G. Ferreira, M. L. Zheludkevich, *Appl. Surf. Sci.* **2020**, 501, 144027.
- [110] P. J. Sideris, U. G. Nielsen, Z. Gan, C. P. Grey, *Science* **2008**, 321, 113.
- [111] G. Yu, F. Hu, H. Huo, W. Ding, L. Peng, *Chem. Phys. Lett.* **2018**, 706, 47.
- [112] G. G. C. Arizaga, A. S. Mangrich, J. E. F. da Costa Gardolinski, F. Wypych, *J. Colloid Interface Sci.* **2008**, 320, 168.
- [113] a) L. Poul, N. Jouini, F. Fiévet, *Chem. Mater.* **2000**, 12, 3123; b) R. Jayashree, P. V. Kamath, *J. Mater. Chem.* **1999**, 9, 961.
- [114] S. Aisawa, J. Sang, Y. Nitani, H. Hirahara, E. Narita, *J. Ceram. Soc. Japan* **2021**, 129, 470.
- [115] T. Sudare, T. Yamaguchi, M. Ueda, H. Shiiba, H. Tanaka, M. Tippoock, F. Hayashi, K. Teshima, *Nat. Commun.* **2022**, 13, 6448.
- [116] M. Henry, J. P. Jolivet, J. Livage, in *Chemistry, Spectroscopy and Applications of Sol-Gel Glasses*, Springer-Verlag, **2006**, pp. 153–206.
- [117] J. Rahbani, N. M. Khashab, D. Patra, M. Al-Ghoul, *J. Mater. Chem.* **2012**, 22, 16361.
- [118] D. O'Hare, J. S. Evans, A. Fogg, S. O'Brien, *Polyhedron* **2000**, 19, 297.
- [119] F. Millange, R. I. Walton, L. Lei, D. O'Hare, *Chem. Mater.* **2000**, 12, 1990.



Zongkun Chen is currently a post-doctoral researcher at the Max Planck Institute for Chemical Energy Conversion in Germany. He received his Ph.D. degree (2020) from the Department of Chemistry at the University of Konstanz. He carried out his post-doctoral research (2020–2021) at the University of Konstanz. His research interests are in the area of crystal growth, the general synthesis of low-dimensional nanomaterials, and the preparation and application of hydroxides.



Qiqi Fan is a Ph.D. student with Professor Helmut Cölfen at the University of Konstanz. Her research interests focus on the design and synthesis of low-dimensional nanomaterials and hydroxides with intercalated anions.



Minghua Huang received her Ph.D. in 2007 from Changchun Institute of Applied Chemistry, CAS. Since 2007, Prof. Huang worked successively as a Humboldt Fellow at the Max-Planck Institute of Colloids and Interfaces, Potsdam, as a research scientist at Leibniz University, Hannover, and as a senior scientist at Ruhr-University, Bochum, Germany. In 2013, she joined Ocean University of China as a Professor in the School of Materials Science and Engineering. Her research interests include the rational design and controlled synthesis of functional nanomaterials as efficient electrocatalysts for ORR and water oxidation, and exploration of the application in renewable energy technologies.



Helmut Cölfen is a full professor of physical chemistry at the University of Konstanz. He received his education and Ph.D. in Chemistry at the Gerhard Mercator University Duisburg. After a postdoctoral stay at the University of Nottingham, he went to the Max-Planck Institute of Colloids and Interfaces in Potsdam as a group leader. From there he changed to the University of Konstanz. His research interests are in the area of nucleation, classical and non-classical crystallization, Biomineralization, synthesis of functional polymers, directed self-assembly of nanoparticles, and fractionating methods of polymer and nanoparticle analysis. He has published more than 440 papers and one book and was listed among the top 100 chemists 2000–2010 by Thomson Reuters and Times Higher Education Index.